FORCES IN ELECTROMAGNETIC DEVICES

B. Aldefeld
Philips GmbH Forschungslaboratorium Hamburg,
D-2000 Hamburg 54

ABSTRACT

For the calculation of total forces in static or dynamic magnetic-field problems, Maxwell's force formula is convenient and generally applicable. A derivation of this formula is given using the idea of Green's equivalent strata, and a number of different practical problems which have been investigated numerically are described.

LIST OF PRINCIPAL SYMBOLS

A	magnetic vector potential	S	surface
B	magnetic flux density	t	time
F,f	force, force density	V	volume
H	magnetic field strength	μ_o	permeability of free space
j	current density		
M	magnetization ($M=B/\mu_o-H$)	μ_r	relative permeability
n	normal vector		
q	hypothetical magnetic charge	ϱ	magnetic pole density

Subscripts

n	normal component
s	surface density
t	tangential component

INTRODUCTION

The operation of many electromagnetic devices depends on the forces acting on conductors and magnetized parts, as in electrical motors, electromagnets, and magnetic levitation systems. In electrical engineering, therefore, the calculation of forces is a subject of great importance.

The treatment of the problem in its general form, which includes the distribution of forces within the material, is of considerable complexity as it involves many different aspects, such as microscopic electrodynamics, elasticity, and thermodynamics. The subject is discussed in several papers, for instance Ref. 1-5, and textbooks [6,7], and a detailed description is given in the book Ref. 8. In most publications, some simplifying assumptions are made, mostly referring to linear or isotropic material, or systems without losses.

In many engineering applications, however, it is only required to know the total forces exerted on moveable parts, while the distribution of the forces within the material is of secondary interest. What is very important, however, is that the effects of nonlinearity and anisotropy, and eddy-current or hysteresis losses in time-varying fields are taken into account.

For such applications, the use of the concept of Maxwell's stresses in empty space offers a convenient way of calculating forces. This method avoids the complicated physics within the material, but is completely general as far as total forces are concerned. The advantages of the method are discussed in the papers of Carpenter[2], Hammond[9] and Carpenter and Ratti[10], where also many practical examples can be found. Further applications are described, for instance, by Reichert et al.[11] and by Kamerbeek[12].

The purpose of this paper is to give a derivation of the force formula and to describe a number of different practical problems which have been investigated numerically. The derivation is based on the idea of Green's equivalent strata, which was also used by other authors[2,9,13], but not described in detail.

DERIVATION OF THE FORCE FORMULA

Consider two nonconnected regions of arbitrary shape, which may represent an electromagnetic device with a movable part. The regions may contain arbitrary distributions of current and magnetization, but the space between the regions is assumed to be empty (Fig. 1). The aim is to derive a formula for the force that the regions exert on each other. The basic equations that will be used in addition to Maxwell's equations for quasistationary fields are

$$d\vec{F} = (\vec{j}\times\vec{B})dV \qquad (1)$$

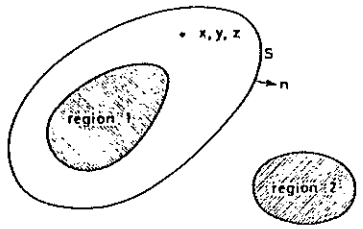

Fig.1. Diagram for deriving the force formula

giving the force on a volume element of current and

$$\vec{F} = q\vec{B} \qquad (2)$$

giving the force on a magnetic pole. (The notion of magnetic poles may be used for mathematical convenience in the calculation of fields and forces if it is assured that the total number of positive poles equals the total number of negative poles, so that a pole can always be regarded as one part of a dipole. As an example, the ends of a long thin solenoid may be considered to represent magnetic poles.)

Field of given sources

According to the Biot-Savart formula extended to the general case where also magnetization is present, the flux density at a point x,y,z is

$$\vec{B} = \frac{\mu_o}{4\pi}\int_{V_1}(\vec{j}+\nabla\times\vec{M})\times\nabla(\frac{1}{r})dV + \frac{\mu_o}{4\pi}\int_{V_2}(\vec{j}+\nabla\times\vec{M})\times\nabla(\frac{1}{r})dV \qquad (3)$$

where r is the distance between the point x,y,z and the position of the volume element dV and each integral represents the contribution from one of the regions. The term ∇xM expresses the fact that a magnetized body produces the same magnetic field as a current with density ∇xM (Ref. 6, Ch. 4.10). The distribution of the magnetization is here assumed to be continuous, which is reasonable since the magnetization at a boundary can always be considered to vary continuously within a small transition layer.

Equivalent sources

An expression equivalent to (3) is

$$\vec{B} = \frac{\mu_o}{4\pi}\int_{V_1}(\vec{j}+\nabla\times\vec{M})\times\nabla(\frac{1}{r})dV - \frac{1}{4\pi}\int_S(\vec{n}\times\vec{B})\times\nabla(\frac{1}{r})dS - \frac{1}{4\pi}\int_S(\vec{n}\cdot\vec{B})\nabla(\frac{1}{r})dS \qquad (4)$$

where S is a surface enclosing region 1 and the point x,y,z (Fig. 1). A method to prove (4) is given in Ref.6, Ch. 4.15, and carried out in the appendix. As a comparison with (3) shows, the volume integral in (4) represents the contribution of region 1, and consequently the two surface integrals represent the contribution of region 2.

The significance of the surface integrals becomes evident when they are compared with the expressions for the fields caused by surface layers of current and magnetic poles: The first surface integral represents the contribution of a surface current of density

$$\vec{j}_s = -\frac{1}{\mu_o}(\vec{n}\times\vec{B}) \qquad (5)$$

since a surface current produces a field

$$\vec{B} = \frac{\mu_o}{4\pi}\int_S \vec{j}_s\times\nabla(\frac{1}{r})dS \qquad (6)$$

analogous to (3). The second surface integral represents the contribution of a surface distribution of poles with density

$$\varrho = -\frac{1}{\mu_o}(\vec{n}\cdot\vec{B}) \qquad (7)$$

since poles distributed over a surface produce a field

$$\vec{B} = \frac{\mu_o}{4\pi}\int_S \varrho\nabla(\frac{1}{r})dS \qquad (8)$$

in analogy to the electrostatic case.

Note that (7) is in accordance with the requirement that magnetic poles must always occur in pairs since integration of (7) over the surface S gives (with the aid of Gauss's divergence theorem)

$$\int_S -\frac{1}{\mu_o}(\vec{n}\cdot\vec{B})dS = \int_V -\frac{1}{\mu_o}\nabla\cdot\vec{B}dV = 0 \quad . \qquad (9)$$

The significance of (4) can therefore be expressed as follows: The field distribution inside a closed surface remains unchanged if the external sources are removed and are replaced by currents and poles on the surface with densities given by (5) and (7) respectively. The equivalent currents and poles are often called Green's equivalent strata after G. Green, whose theorem is used to derive the expression (4).

While the equivalent sources do not change the field inside S, they reduce the field to zero outside S. This follows from the fact that a current layer gives rise to a discontinuity in the tangential field component of magnitude

$$\vec{n}\times(\vec{B}_2-\vec{B}_1) = \mu_o\vec{j}_s \qquad (10)$$

(Ref. 6, Ch. 4.12), where the subscripts 1 and 2 refer to the flux density immediately inside and outside the surface respectively, and a pole layer leads to a discontinuity in the normal field component of magnitude

$$(\vec{B}_2-\vec{B}_1)\cdot\vec{n} = \mu_o\varrho \qquad (11)$$

(Ref. 6, Ch. 3.15). From (5) and (10) it follows then that

$$\vec{n} \times (\vec{B}_2 - \vec{B}_1) = -\vec{n} \times \vec{B}_1 \qquad (12)$$

and from (7) and (11)

$$(\vec{B}_2 - \vec{B}_1) \cdot \vec{n} = -\vec{n} \cdot \vec{B}_1 \quad . \qquad (13)$$

Equations (12) and (13) state that the field is zero immediately outside the surface S, and consequently it must be zero everywhere outside S since in the equivalent model no sources exist in that region.

Forces

Since forces can only be transmitted via the electromagnetic field, it is obvious that the equivalent layers must exert the same forces on region 1 as the original sources they replace. Further, as follows from the principle "action = reaction", this force must be equal to the force which the sources within region 1 exert on the equivalent layers, and this force can now easily be computed. For that purpose, it is helpful to consider the current and pole layers to be separated by a very small distance and also to consider the layers to have a small thickness. Then, the components of the flux density vary linearly within the layer. Figure 2 illustrates the conditions at the surface S.

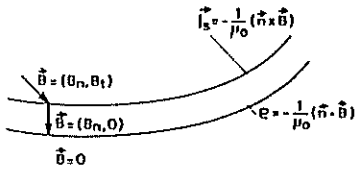

Fig. 2. Flux density and equivalent sources at the surface S

The force density (force per unit area) on the current layer is according to (1) and (5)

$$\vec{f}_c = -\frac{1}{\mu_o}(\vec{n} \times \vec{B}) \times (B_n, \tfrac{1}{2} B_t) \qquad (14)$$

where the factor 1/2 is due to the fact that the tangential component of $\vec{B}$ decreases to zero across the current layer. Correspondingly, the force density on the pole layer is according to (2) and (7)

$$\vec{f}_p = -\frac{1}{\mu_o}(\vec{n} \cdot \vec{B}) \; (\tfrac{1}{2} B_n, \; 0) \quad . \qquad (15)$$

The total force density is given by the sum of (14) and (15), which by means of the vector identity

$$(\vec{a} \times \vec{b}) \times \vec{c} = \vec{b}(\vec{c} \cdot \vec{a}) - \vec{a}(\vec{c} \cdot \vec{b}) \qquad (16)$$

can be transformed to

$$\vec{f}_c + \vec{f}_p = -\frac{1}{\mu_o} \vec{B}(\vec{B} \cdot \vec{n}) + \frac{1}{2\mu_o} B^2 \vec{n} \; . \qquad (17)$$

The total force is obtained by integrating this expression over the surface S, and the total force on region 1 is given by the negative of that expression, so that the final result is

$$\vec{F} = \int_S [\frac{1}{\mu_o} \vec{B}(\vec{B} \cdot \vec{n}) - \frac{1}{2\mu_o} B^2 \vec{n}] dS \; . \qquad (18a)$$

The integrand in (18a) can be split up into the components of the force density normal and tangential to the surface, which gives

$$f_n = \frac{1}{2\mu_o} (B_n^2 - B_t^2) \qquad (18b)$$

$$f_t = \frac{1}{\mu_o} B_n B_t \qquad (18c)$$

where the tangential component has the direction of B_t. These functions are illustrated in fig. 3. The total torque exerted on region 1 is

$$\vec{T} = \int_S [\frac{1}{\mu_o}(\vec{r} \times \vec{B})(\vec{B} \cdot \vec{n}) - \frac{1}{2\mu_o} B^2 (\vec{r} \times \vec{n})] dS \qquad (19)$$

The forces given by (18) are equivalent to the so-called Maxwell's stresses in vacuum. These stresses

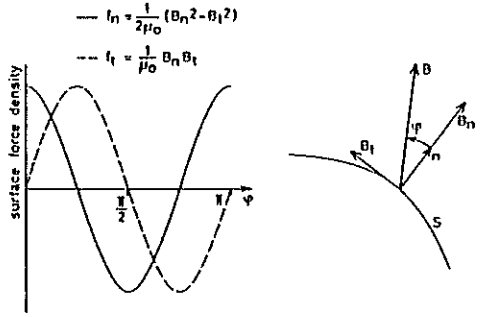

Fig. 3. Components of the force density as functions of φ

consist of a tension of magnitude $B^2/(2\mu_0)$ along the flux lines and a pressure of $B^2/(2\mu_0)$ perpendicular to the flux lines. The equivalence with (18) follows immediately when (18) is applied to surfaces parallel and perpendicular to the flux lines.

It should be mentioned that the forces transmitted by electrical fields are given by expressions that are analogous to (18), with the magnetic flux density vector replaced by the electrical displacement vector and the permeability of free space replaced by the permittivity of free space. In most practical cases, however, these forces are by orders of magnitude lower than the magnetic forces.

Remarks

1. The equations (18) and (19) give the magnetic force and torque on any movable part if the flux density distribution is known over a surface enclosing the part. Note that the field sources need not be known for the evaluation.
2. The force densities given by 18b,c may not be interpreted as actual force densities acting on the surface, but as force densities that are transmitted across the surface.
3. The surface of integration may be arbitrarily chosen. However, it must envelop the part under consideration completely and may not intersect other parts.
4. If the surface of integration is coincident with an iron surface and the iron is not saturated, the tangential component of the flux density is zero, so that only the normal component of the force density need be taken into account. In cases where the iron is highly saturated, however, the contribution of the tangential component can be comparable to that of the normal component or even be higher (see below).
5. Since no assumptions have been made in the derivation of the formula about the nature of the sources within the closed surface, the formula is generally valid. In particular, the enclosed region may contain arbitrary distributions of eddy currents, moving parts, and materials with nonlinear or anisotropic characteristics. A point of theoretical interest is that the electromagnetic field itself has a momentum (Ref. 6, Ch. 2.6), which was neglected in the derivation of the force formula. For practical applications, however, this momentum is by far too small to be of any importance.

NUMERICAL INVESTIGATIONS

Illustrative examples

Figure 4 shows the flux lines of a long solenoid, which produces a field approximating that of two magnetic

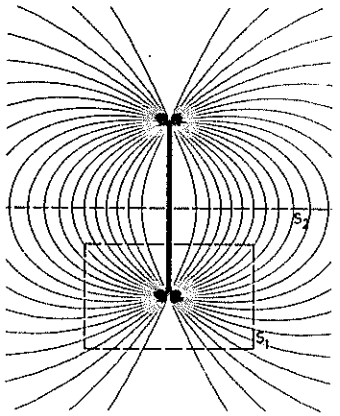

Fig.4. Long solenoid

poles of opposite sign. To calculate the force which one pole exerts on another one, any surface enclosing one pole can be chosen, for instance that denoted by S_1 in Fig. 4. Another possible choice is denoted by S_2. This surface is assumed to extend sufficiently far to the region of low magnetic field intensity. Since the two poles are assumed to be separated in this model, the small circular element where the solenoid intersects the surface must be omitted from the integration.

For such a solenoid, the force can also be calculated analytically by a simple expression based on (2), and this can be used to check the numerical calculation. For the solenoid shown in Fig. 4 the agreement was found to be within 1%, the small difference being due to the discretization error in the numerical solution and to the assumption of infinitesimal diameter in the analytical solution.

A similar example is given in Fig. 5, which shows the flux lines of two parallel current-carrying conductors with very small diameter and two possible choices for the surface of integration. This case, too, can be treated analytically by simply applying Ampere's law to obtain the magnetic field of one conductor and

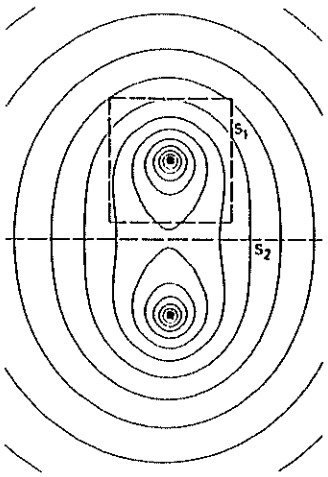

Fig.5. Parallel current-carrying conductors

using (1) to calculate the force on the other conductor.

An important point to note is that the use of different surfaces in a single field calculation can be used as criterium to check the consistency of the results. Marked differences in the forces can indicate that the magnetic field solution has not converged sufficiently, or that the finite-element net has not been set up adequately.

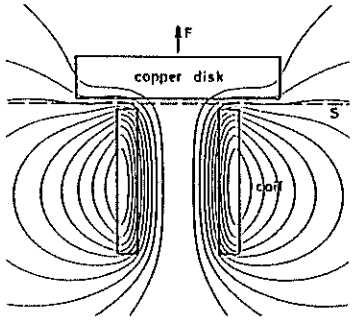

Fig.6. Levitated copper disk

An example for the application of the force formula in an eddy-current problem is given in Fig. 6, which shows a copper disk that is levitated by the forces on the eddy currents induced by a rapidly varying applied field. A point to note is that the eddy currents influence the magnetic field, of course, but their distribution need not explicitly be known for the calculation of the forces.

Small air gaps

If an electromagnetic device consists of several parts, it is sometimes required to know the force on each part, so that, if necessary, appropriate means of preventing disruption of the parts can be devised. From the preceding sections it is clear that these forces can very easily be obtained by the application of (18) if each

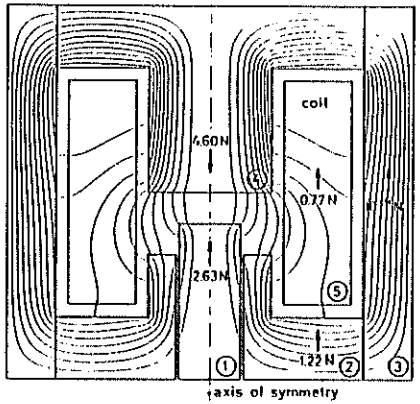

Fig.7. Balance of forces in an electromagnet

part is enclosed by a surface, which, for instance, may follow directly the contour of the parts. An example is given in Fig. 7, which shows the numerically calculated flux lines and the forces within a simple plunger-type electromagnet. As the balance requires, the sum of all the forces is zero within a certain accuracy.

A fact that can give rise to difficulties in the numerical calculation is that the air gaps can sometimes be extremely small, for instance if two parts are in contact, as is assumed in the electromagnet of Fig. 7 for parts 2 and 3, and 3 and 4. In order to satisfy the precondition of (18), it seems to be reasonable to assume that a very small air gap exists between the parts. This, however, can adversely affect the convergence or stability of the numerical solution. One point is that very large differences in the spacing of the discretization net can impede the convergence of itera-

tive solutions. Another point is that such large differences can cause round-off errors of considerable magnitude.

The problem can be solved easily, however, if the air gap is so small that it has only negligible influence on the field distribution. In that case, the air gap can be omitted in the numerical solution, since the required values of the flux density follow immediately from the continuity of B_n and H_t. These values are $B_n(\text{air})=B_n$ and $B_t(\text{air})=B_t/\mu_r$, so that (18a,b) transform to

$$f_n = \frac{1}{2\mu_o}\left(B_n^2 - \frac{B_t^2}{\mu_r^2}\right) \qquad (20a)$$

$$f_t = \frac{1}{\mu_o\mu_r} B_n B_t \quad . \qquad (20b)$$

These expressions can be used for any closed surface, but the result must be interpreted as the total force that would be exerted on the enclosed part if it were separated from the other parts by a very small air gap.

Pole tips

A problem of much practical interest is the calculation of forces in geometries with pole tips. Such geometries are important in some types of rotating machines and electromagnets, for instance. Many details of this problem have been discussed by Byrne and O'Connor[14]. An aspect that shall be emphasized here concerns the pronounced concentration and inhomogeneity of the field that can occur.

As an example, Fig. 8 and 9 show the magnetic

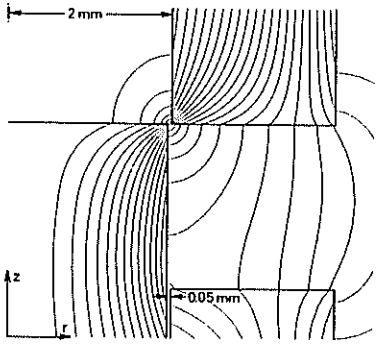

Fig 8. Flux lines in pole tip region at low field intensity

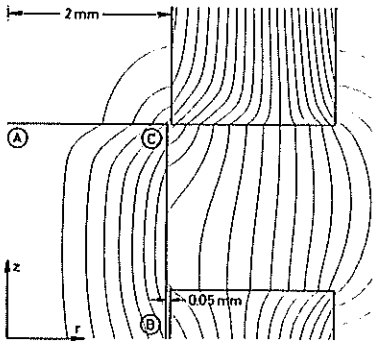

Fig 9. Flux lines in pole tip region at high field intensity

field near the pole tips in a plunger-type electromagnet at low and high field intensity respectively. Clearly, the air region between the tips is the most critical for the force calculation since it contributes the main part to the surface integral. The consequence is that this region must be subdivided into very small elements for the numerical solution. (Since near pole tips a considerable amount of field energy is stored, the discretization of such a region is critical not only for the forces but also for the field distribution within the whole geometry.) In the highly saturated case shown in Fig. 9, where the permeability near the pole tips approaches that of air, the effect of field concentration is less pronounced.

Fig. 10 shows the distribution of the force density for the field configuration of Fig. 9 along AC and BC. In this example it is assumed that only the z-component of the force is of interest, so that along

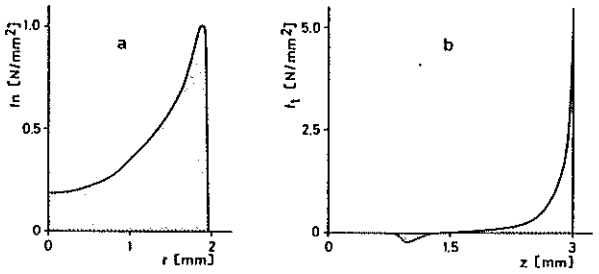

Fig.10. Z-component of force density along AC and BC (Fig 9)
a) normal component along AC b) tangential component along BC

AC only the normal component and along BC only the tangential component is given. The remarkable facts are that both contributions are comparable and that the tangential component is concentrated in a small region near the pole corners.

Magnetic field diffusion

An important topic in magnetodynamic problems is the diffusion of the magnetic field in ferromagnetic materials. What is of interest in the present context is how the diffusion process determines the way in which the forces are transmitted. The example used to illustrate this concerns the semi-infinite ferromagnetic space under the excitation of a tangential surface field H_o (Fig. 11). This field is assumed to vary like a step pulse ($H = 0$ for $t \leq 0$, $H = H_o$ for $t>0$) and to be of such intensity that the material is strongly saturated.

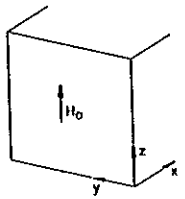

Fig 11. Geometry used in diffusion example

The easiest way to treat this problem is by means of the simplified theory first used by Rosenberg[15] for sinusoidal excitation. In this theory it is assumed that due to the strong saturation a flux density wave of rectangular shape moves into the material. From Maxwell's equations it follows then that the eddy-current density has also rectangular shape and that the magnetic field intensity varies linearly between the surface and the position of the wave front, where it is zero.

This behaviour is illustrated in Fig. 12 for $t = 0.4$ ms and $H_o = 5\times10^4$ A/m. Instead of H the expression $1/2\ \mu_o H^2$ is shown, which according to (18b) can be regarded to describe the magnitude of the force density transmitted across a plane parallel to the surface. The practical meaning is that if a small cut were made parallel to the surface, this force density would be measured. (H is not affected by such a cut.) For comparison, Fig. 13 shows the same behaviour calculated numerically using an actual magnetization curve.

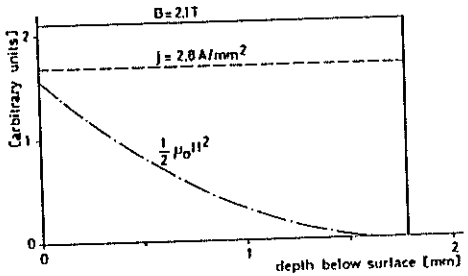

Fig 12. Field diffusion under step excitation (t = 0.4 ms, Rosenberg's theory)

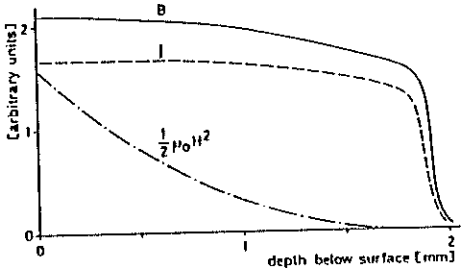

Fig 13. Field diffusion under step excitation (t = 0.4 ms, numerical solution)

The time dependence and the variation with the physical properties of the material follow from the simplified theory as

$$d(t) = \sqrt{\frac{2H_o t}{\sigma B}} = \sqrt{\frac{2t}{\sigma H_o \mu_r(H_o)}} \qquad (21)$$

where d is the position of the wave front and σ denotes the electrical conductivity of the material. The evaluation of (21) for different materials shows that d and hence also the velocity with which the force is transmitted depend strongly on the properties of the material. An important consequence of this fact for a class of practical applications will be described in the next section.

Fast-acting devices

In many relay applications or in high-speed electromagnetic actuators, the speed of the moving parts and high repetition rate are of prime interest. As to the forces, this means that they should not only be as high as possible, but also that there should be little delay between the excitation and the generation of the forces. The first of these requirements is usually met by choosing a magnetic material with high saturation flux density and the second by using laminated or slotted material in order to suppress the eddy currents. Laminated or slotted material, however, can sometimes not be used because of technological difficulties and resulting excessive costs, as in some devices of very small dimensions, for instance. In those cases, an important factor determining the choice of the material is the velocity with which the magnetic field can diffuse in the material. As a basis for an estimation, equation (21) can be very helpful, but the actual geometry modifies that simple relationship, so that numerical calculations are necessary to obtain more precise knowledge.

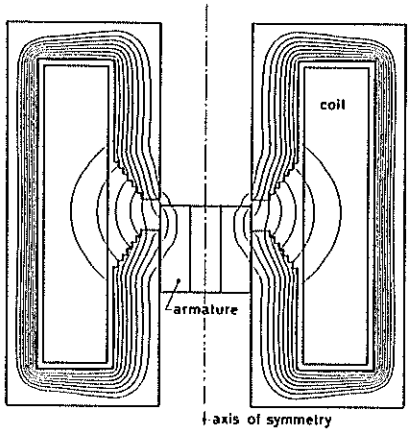

Fig.14. Penetrating flux wave in fast-acting electromagnet

Examples for such calculations are illustrated in Fig. 14 to 16, which apply to an electromagnet with movable armature under step excitation. Figure 14 shows the computed flux lines during the diffusion process at a time when the flux wave has not yet fully penetrated the material. Figure 15 shows the time variation of the force exerted on the armature and the influence of material properties. For the iron used, the saturation flux density is 2.15 T and the electrical conductivity

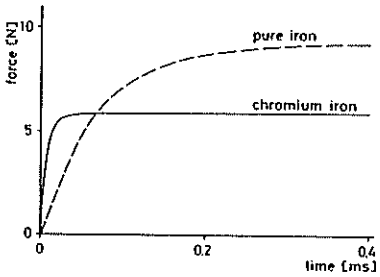

Fig.15. Force on the armature of the electromagnet shown in Fig.14 with different materials

is 6×10^6 S/m, and for the chromium iron these values are 1.7 T and 7×10^5 S/m respectively. The important point shown in Fig. 15 is that the suitable choice of the material depends strongly on the desired rise time of the force. Another important fact is that with increasing saturation a shorter rise time of the force is obtained (Fig. 16). This follows from equation (21), which gives a higher velocity of field penetration for decreasing permeability. In high-speed devices, therefore, strong saturation is necessary for maximum speed.

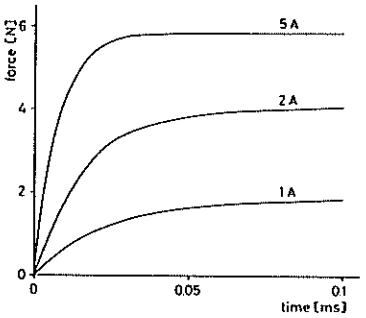

Fig.16. Force on the armature of the electromagnet shown in Fig.14 with different excitation currents (material: chromium iron)

ACKNOWLEDGEMENTS

The numerical examples in this paper were calculated using the computer program EDDY, the development of which was sponsored by the German Federal Ministry for Research and Technology (BMFT) under grant HH-PHI/103.

REFERENCES

1. Byrne, J. V., Forces in saturable electromechanical devices, Ph. D. thesis, University College Dublin, 1973.
2. Carpenter, C. J., Surface-integral methods of calculating forces on magnetized iron parts, Proc. IEE, Vol. 107C, 19-28, 1960.
3. Carter, G. W., Distribution of mechanical forces in magnetized material, Proc. IEE, Vol. 112, 1771-1777, 1965. Discussion: ibid, Vol. 113, 2095-2098, 1966; ibid. Vol. 113, 401-402, 1966; ibid., Vol. 113, 719-720, 1966.
4. Chu, L. J., Haus, H., A., and Penfield, P., The force density in polarizable and magnetizable fluids, Proc. IEEE, Vol. 54, 920-935, 1966.
5. Slepian, J., Electromagnetic ponderomotive forces within material bodies, Proc. Nat. Acad. Sci., Vol. 36, 485-497, 1950.
6. Stratton, J. A., Electromagnetic theory, McGraw-Hill, New York and London, 1941.
7. Woodson, H. H. and Melcher, J. R., Electromechanical dynamics, John Wiley, New York 1968, Part II.
8. Birrs, R. R., Electric and magnetic forces, Longmans, 1967.
9. Hammond, P., Forces in electric and magnetic fields, Bull. Elect. Eng. Educ., Vol. 25, 17-28, 1960.
10. Carpenter, C. J. and Ratti, U., Calculation of mechanical forces in electrical machines by surface integration, L'Energia Elettrica, N. 5, 254-262, 1974.
11. Reichert, K., Freundl, H., und Vogt, W., The calculation of forces and torques within numerical magnetic field calculation methods, COMPUMAG Conference on the computation of magnetic fields, Oxford, 64-73, 1976.
12. Kamerbeek, E. M. H., On the theoretical and experimental determination of the electromagnetic torque in electrical machines, Philips Res. Rept. Suppl., No. 4, 1970.
13. Heaviside, O., Electrical papers, McMillan, 1892, Articles 23 and 52.
14. Byrne, J. V. and O'Connor, W. J., Saturable overlapping rectangular poles, IEEE Trans., Vol. MAG. 11, 1547-1569, 1975.
15. Rosenberg, E., Wirbelströme in massivem Eisen, Elektrotechn. Z., Vol. 44, 513-518, 1923.

APPENDIX

Derivation of equation (4)

Stratton (Ref. 6, Ch. 4.14) has shown that the vector analogue of Green's theorem is

$$\int_V (\vec{Q}\cdot\nabla\times\nabla\times\vec{P}-\vec{P}\cdot\nabla\times\nabla\times\vec{Q})dV = \int_S (\vec{P}\times\nabla\times\vec{Q}-\vec{Q}\times\nabla\times\vec{P})\cdot\vec{n}dS \qquad (A1)$$

where $\vec{P}$ and $\vec{Q}$ are vector functions of position and V is a region bounded by the surface S.

Let $\vec{P}$ represent the vector potential $\vec{A}$, which satisfies the differential equation

$$\nabla\times\nabla\times\vec{A} = \mu_o(\vec{j}+\nabla\times\vec{M}) \qquad (A2)$$

and let $\vec{Q}$ represent the function defined by

$$\vec{Q} = \nabla(\frac{1}{r})\times\vec{a} = \nabla\times\frac{\vec{a}}{r} \qquad (A3)$$

where $\vec{a}$ is an arbitrary constant vector and r is the distance between a point x,y,z within S and the position of the volume or surface element.

Using the vector identity

$$\nabla\times\nabla\times\vec{b} = \nabla(\nabla\cdot\vec{b})-\nabla^2\vec{b} \qquad (A4)$$

and because

$$\nabla^2\frac{\vec{a}}{r} = 0 \qquad (A5)$$

we obtain

$$\nabla\times\vec{Q} = \nabla\times\nabla\times\frac{\vec{a}}{r} = \nabla(\vec{a}\cdot\nabla(\frac{1}{r})) \qquad (A6)$$

and

$$\nabla\times\nabla\times\vec{Q} = \nabla\times\nabla(\vec{a}\cdot\nabla(\frac{1}{r})) = 0 \ . \qquad (A7)$$

Substituting (A2), (A6), and (A7) in (A1) gives

$$\mu_o\int_V(\nabla(\frac{1}{r})\times\vec{a})\cdot(\vec{j}+\nabla\times\vec{M})dV =$$

$$\int_S[\vec{A}\times\nabla(\vec{a}\cdot\nabla(\frac{1}{r}))]\cdot\vec{n}dS + \int_S[(\vec{a}\times\nabla(\frac{1}{r}))\times(\nabla\times\vec{A})]\cdot\vec{n}dS \ . \qquad (A8)$$

The first integrand on the right-hand side can be written

$$\vec{A}\times\nabla(\vec{a}\cdot\nabla(\frac{1}{r})) = -\nabla\times(\vec{A}\vec{a}\cdot\nabla(\frac{1}{r}))+\vec{a}\cdot\nabla(\frac{1}{r})(\nabla\times\vec{A}) . \quad (A9)$$

The application of Gauss's theorem shows that the integration over the first term gives zero since $\nabla\cdot(\nabla\times\vec{b})=0$ for any vector $\vec{b}$. Using this, replacing $\nabla\times\vec{A} = \vec{B}$, and applying the identities

$$(\vec{b}_1\times\vec{b}_2)\cdot\vec{b}_3 = (\vec{b}_2\times\vec{b}_3)\cdot\vec{b}_1 = (\vec{b}_3\times\vec{b}_1)\cdot\vec{b}_2 \quad (A10)$$

$$(\vec{b}_1\times\vec{b}_2)\cdot(\vec{b}_3\times\vec{b}_4) = \vec{b}_1\cdot[(\vec{b}_2\times(\vec{b}_3\times\vec{b}_4)] \quad (A11)$$

(A8) can be transformed to

$$\mu_o\int_V(\vec{j}+\nabla\times\vec{M})\times\nabla(\frac{1}{r})dV = \int_S(\vec{n}\cdot\vec{B})\nabla(\frac{1}{r})dS+\int_S(\vec{n}\times\vec{B})\times\nabla(\frac{1}{r})dS. \quad (A12)$$

Since the function $\vec{Q}$ has a singularity at r = 0, (A12) is not valid for that point, so that it must be excluded. Therefore, let that point be enclosed by a small sphere with surface S_1 and let the corresponding surface integrals

$$I = \int_{S_1}(\vec{n}\cdot\vec{B})\nabla(\frac{1}{r})dS + \int_{S_1}(\vec{n}\times\vec{B})\times\nabla(\frac{1}{r})dS \quad (A13)$$

be added to (A12). The integrand in the second term in (A13) can be transformed to

$$(\vec{n}\times\vec{B})\times\nabla(\frac{1}{r}) = \vec{B}\times(\nabla(\frac{1}{r})\times\vec{n}) + \vec{B}(\vec{n}\cdot\nabla(\frac{1}{r})) -\nabla(\frac{1}{r})(\vec{n}\cdot\vec{B}) . \quad (A14)$$

The first term in (A14) is zero because $\nabla(\frac{1}{r})$ and $\vec{n}$ have the same direction, and the last term cancels the first term in (A13), so that the surface integral over the sphere is

$$I = \int_{S_1}\vec{B}(\vec{n}\cdot\nabla(\frac{1}{r}))\,dS . \quad (A15)$$

With

$$\nabla(\frac{1}{r}) = \frac{1}{r^2}\frac{\vec{r}}{r} \quad (A16)$$

and $r \to 0$ the integral (A15) reduces to

$$\int_{S_1}\vec{B}(\vec{n}\cdot\frac{1}{r^2}\frac{\vec{r}}{r})dS = \int_{S_1}\vec{B}\,\frac{1}{r^2}\,dS = 4\pi\vec{B} . \quad (A17)$$

Adding (A17) to (A12) and rearranging gives the final result

$$\vec{B} = \frac{\mu_o}{4\pi}\int_V(\vec{j}+\nabla\times\vec{M})\times\nabla(\frac{1}{r})dV - \frac{1}{4\pi}\int_S(\vec{n}\cdot\vec{B})\nabla(\frac{1}{r})dS - \frac{1}{4\pi}\int_S(\vec{n}\times\vec{B})\times\nabla(\frac{1}{r})dS . \quad (A18)$$

AUTOMATIC PLANNING OF ELECTRICAL OR MAGNETIC EQUIPMENT STARTING FROM THE STUDY OF FIELDS (*)

A. Di Napoli - C. Mazzetti - M. Mele
Electrical Institute, University of Rome

ABSTRACT

In this work, the Authors set out a method for the automatic planning of the shape and size of electrical or magnetic equipment, either in the presence of a high flux, or whenever the potential on the boundary must assume some pre-established values. The method is developed if the system is regulated by the Laplace's and/or Poisson's equation, and the study is carried out making use of a calculation program, developed by the Authors, that utilizes the finite-element numerical method.

1. FORMULATION OF THE PROBLEM

The study of fields may be used either as a direct analysis and verification method for the calculation of potential throughout the region occupied by the electrical and/or magnetic system, or as a method of synthesis and, hence, of project.
In this work, the Authors set out a method for the automatic planning of the shape and size of electrical or magnetic equipment. This method is based on the condition that the electrical or magnetic field on some areas of the boundary does not exceed some pre-fixed values, or that the electric or magnetic potential in some areas surrounding the structure realizes such a behaviour as to allow a correct operation of the said equipment.
The approach is developed in the case in which the system is regulated by Laplaces' and/or Poisson's equation, and the study is carried out using a calculation program, developed by the Authors, that utilizes the finite-element numerical method[1].
Substantially, the point is to obtain the coordinates of points located along a boundary or along a surface between two materials with different dielectric or magnetic characteristics, in such a way that not only the boundary conditions sufficient for the solution of the direct problem are verified, but also further conditions are verified that are dictated by well-defined technical opportunities.
Table I shows, by way of exemplification, some electrical and magnetic problems with the relevant project conditions
Later in this study, the applications relative to the magnetic field will be developed, in the assumption of identifying in the system a plane or cylindrical symmetry, in such a way that the problem may be considered of the two-dimensional type.

(*) This work was sponsored by the Italian Research Council (CNR, Rome, Italy).

TABLE I

problem	project condition	
1) shape of the pole surface	magnetic induction of such a value as to prevent the iron from working in the saturation area	$B < B_s$
2) shape of the pole surface	sinusoidal distribution of the magnetic induction in the air gap along a polar pitch of a lenght 2l	$A(x) = A_M \sin \frac{\pi}{2l} x$
3) H.V. electrodes	electrical field all along the surface of the electrode, whose value is lower than the critical discharge gradient (E_c)	$E < E_c$
4) H.V. dividers	linear distribution of the electrical potential along the high voltage column of the lenght l divider	$V(x) = \frac{x}{l} V(l)$

In final words, the compliance with well-defined technical conditions on the potential and on the field, is the further constraint that allows to obtain equation $y = f(x)$ of the curve that represents the unknown quantity of the problem: for example, the size of the magnetic pole or that of the high voltage electrode.

2. DESCRIPTION OF THE METHOD

The method used for defining an unknown boundary is of the iterative type[2,3]. In the region under review, the coordinates of the points whose position is not known, are initially fixed in a congruent manner to the problem under examination, in order to make the convergence to the solution quicker.
It is necessary to discretize the region under examination into triangular elements in such detail as would be required to study; the values are thus calculated of the electrical or magnetic potential in all the points considered, that are linked to the respective flux densities by the following relations:

$$\overline{E} = - \text{grad } V \qquad (1)$$

$$\overline{B} = \text{rot } \overline{A} \qquad (2)$$

Relations (1) and (2), in the assumption of considering the system

two-dimensional, particularize as follows:

$$E_x = -\frac{\partial V}{\partial x}\ ; \qquad E_y = -\frac{\partial V}{\partial y} \qquad (3)$$

$$B_x = \frac{\partial A_z}{\partial y}\ ; \qquad B_y = -\frac{\partial A_z}{\partial x} \qquad (4)$$

In the plane case, there exists, therefore, for the magnetic potential, only the component along this plane (A_z), and therefore, the differential relations (3) and (4), linking the electrical or magnetic potential to the respective fields, are of the same shape.
If we thus indicate by D the electric or magnetic fields, and by P the respective potential, these equations may be shown, from the numerical viewpoint, in the generalized form:

$$D_x = \{f_i(x,y)\} \quad \{P_i\} \qquad (5)$$

$$i=1,2...n$$

$$D_y = \{g_i(x,y)\} \quad \{P_i\} \qquad (6)$$

where P_i represents the potential vector in the nodes of each triangular element, and f_i and g_i are the matrix function, according to the finite element discretization.
If the elements considered are of the first order, equations (5) and (6) become linear combinations, whose coefficients, of the type $b_i = y_j - y_k$ or $c_i = x_k - x_j$, are the difference between the coordinates of the three nodes of the triangle under examination.
With 2nd order elements discretization, functions f and g are expressed themselves through 2nd degree forms, in which there still appear the coordinates x_i and y_i of the six nodes of the parabolic triangle.
If we indicate by D_n and D_t the components of vectors normal flux densities and tangential to the unknown profile, for each node 'h' laying in it, the following shall apply:

$$D_{nh} = D_x \frac{(y_h - y_{h-1})}{\sqrt{(y_h-y_{h-1})^2+(x_h-x_{h-1})^2}} - D_y \frac{(x_h - x_{h-1})}{\sqrt{(y_h-y_{h-1})^2+(x_h-x_{h-1})^2}} \qquad (7)$$

$$D_{th} = D_x \frac{(x_h - x_{h-1})}{\sqrt{(y_h-y_{h-1})^2+(x_h-x_{h-1})^2}} + D_y \frac{(y_h - y_{h-1})}{\sqrt{(y_h-y_{h-1})^2+(x_h-x_{h-1})^2}} \qquad (8)$$

From equations (5) and (6) we get D_x and D_y in equations (7) and (8), to obtain the functions of the geometrical coordinates of the nodes of the unknown profile and of the corresponding potentials.

If we introduce the project condition in the first member of relations (7) and (8), the equation in general will not be verified by the values of the starting profile coordinates.
In this case, relations (7) and (8) will be solved by expressing coordinates x_h and y_h as unknown quantities, thus obtaining new values for the coordinates of the profile nodes. The values thus obtained are utilized for a successive iteration cycle, which starts by once again solving Laplace's or Poisson's equation, to obtain the new potential values throughout the region considered.
The procedure terminates whenever, in equations (7) and (8), after substituting the project conditions for their first member, x_h and y_h coordinates are such as to result in identities within the scope of the desired accuracy. In this case, the values of coordinates x_h and y_h in between two iterations will cease to show appreciable variations and will therefore identify the desired profile representing the solution of the problem.
It should be observed that in assigning the conditions imposed by the project, two cases must be distinguished, as follows:

1) the project condition is assigned with a condition on the electrical magnetic field in the area adjacent to the unknown profile, as in problems 1) and 3) of Table I. In this case, the problem can be directly solved by introducing the project values D_{nh} and D_{th} into equations (7) and (8), and then proceeding in the above indicated manner.

2) the project condition is assigned on the electrical and magnetic potential in a part of the boundary different from the unknown profile, as in problems indicated by 2) and 4) in Table I. In this case, it is necessary to preliminarily calculate D_{nh} and D_{th} values along the profile, solving the direct electromagnetic problem with the boundary conditions imposed by the project. Once such values are known for each iteration cycle, they are replaced as first member of (7) and (8), proceeding in the known manner.

3. ANALYSIS OF RESULTS

Problem N. 1

Fig. 1 emphasizes the geometry and boundary conditions relative to the magnetic problem 1), as expressed in Table I. Three distinct regions may be distinguished in the region under examination: a first one in iron, the second one in air, regulated by Laplace's equation, the third occupied by the electrical windings and regulated by Poisson's equation.
The project condition referred to in Table I, is imposed on the magnetic induction in the region adjacent to the pole profile in the region occupied by the iron. The induction value is chosen in such a way as to cause the ferromagnetic system to work in the linear section of its characteristic; it ensues that Laplace's equation still results to be linear.
Fig. 2 shows the discretization of the integration field by means of finite elements of the first order; it is necessary to discretize in such detail as would be required by the curvature profile.

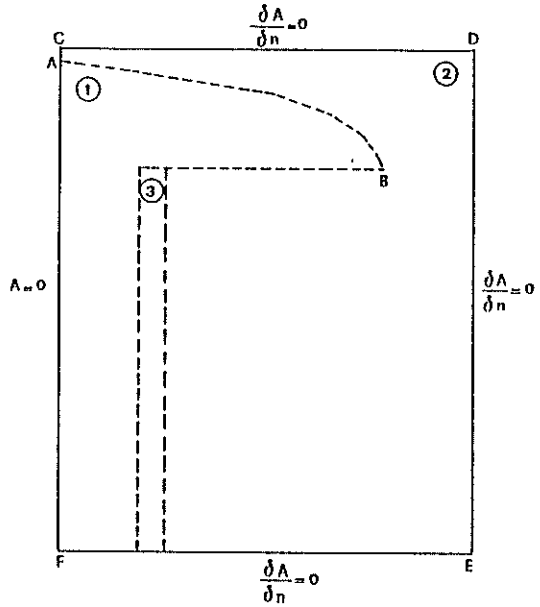

Fig. 1 - Problem n. 1: geometry and boundary conditions.
1) Iron
2) air
3) winding
DE: Inter-polar axis

By imposing two different values of magnetic induction, the two corresponding profiles shown in Fig. 3 were calculated according to the procedure described in the previous paragraph.
Fig. 4 shows the unknown profile that is obtained for an established magnetic induction value (B = 1,2 Wb/m^2) in correspondence of different iteration cycles, starting from the initially established profile.

Problem N. 2

Concerning the magnetic problem N. 2 of Table I, an integration domain was taken into examination, that excludes the zone in iron, the saturation problem not being now considered. Fig. 5 clearly shows the boundary conditions for this domain.
The project condition is imposed on the potential vector A, which, along the center line of the air gap (segment CD of fig. 5), assumes a sinusoidal behaviour-trend, whose maximum value is calculated in the following manner.
The value is first established of the current density flowing in the winding, and then the potential distribution along the air-gap center line is calculated by solving Poisson's equation; and finally, the flux linking with the winding itself.

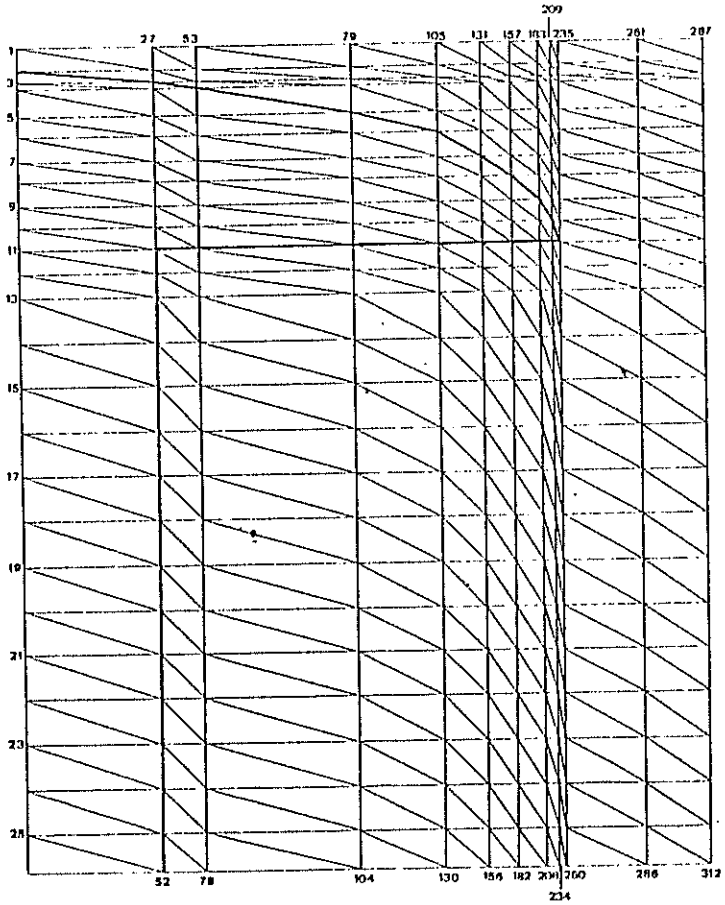

Fig. 2 - Trinagular discretization with first order elements.

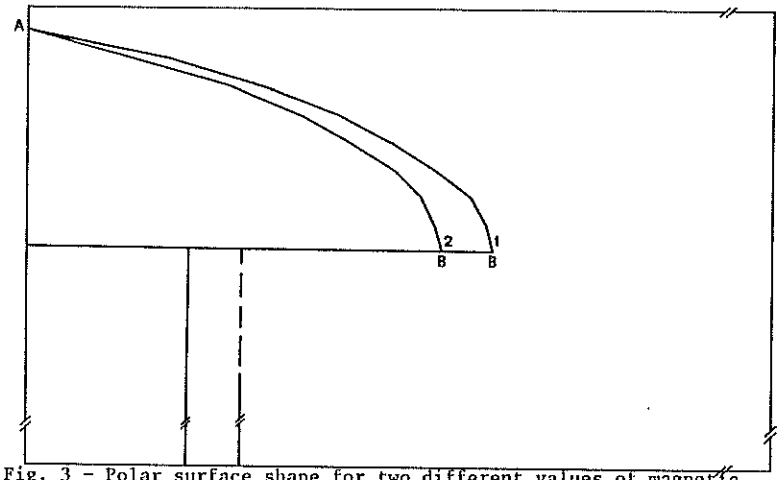

Fig. 3 - Polar surface shape for two different values of magnetic induction:
1) - B = 1,4 Wb/m^2
2) - B = 1,3 Wb/m^2

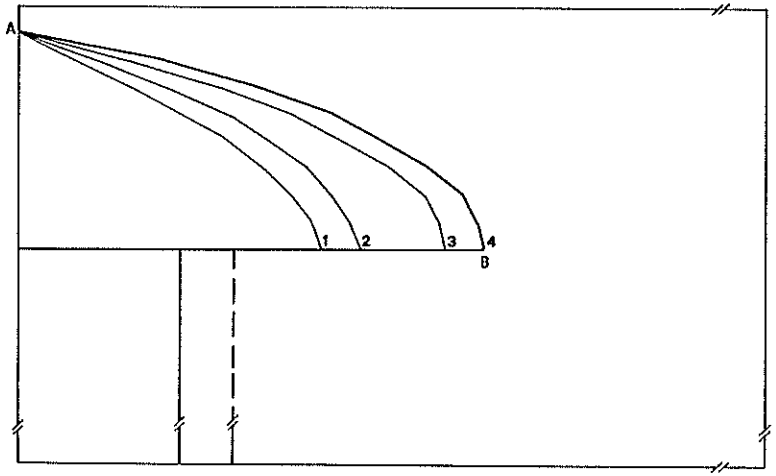

Fig. 4 - Polar surface shape at different iteration cycles:
1) initial profile
2) profile after three iteration cycles
3) profile after seven iteration cycles
4) profile after eleven iteration cycles.

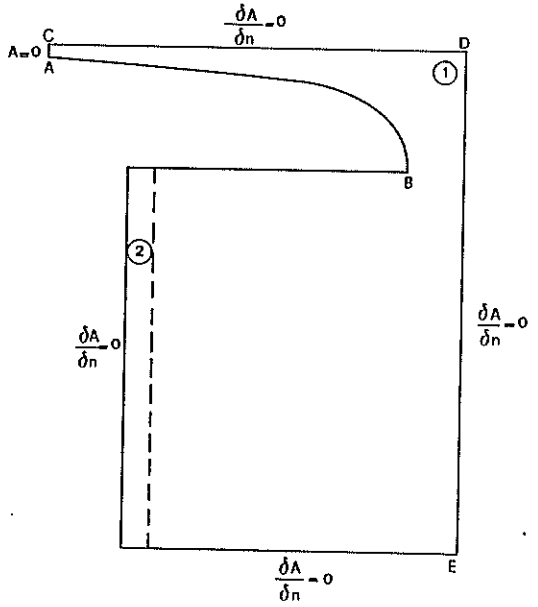

Fig. 5 - Problem n. 2: geometry and boundary conditions
1) air
2) winding

Such a distribution will not result to be, as a rule, sinusoidal, but in the assumption that the flux should remain constant whatever the potential vector distribution may be, the maximum value of the sinusoidal distribution can be calculated by means of the following relation:

$$A_M = \frac{\Pi}{2\ 1} \int_0^1 A(x)\ d\ x \qquad (9)$$

being 1 the lenght of segment CD.
Fig. 6 shows the shape of the pole surface automatically obtained according to the method illustrated above, assuming three different values of the current density in the winding.
Fig. 7 shows the unknown profile that is obtained for an established current density value (J = 1,2 A/mm^2) at different iteration cycles starting from the initially fixed profile.

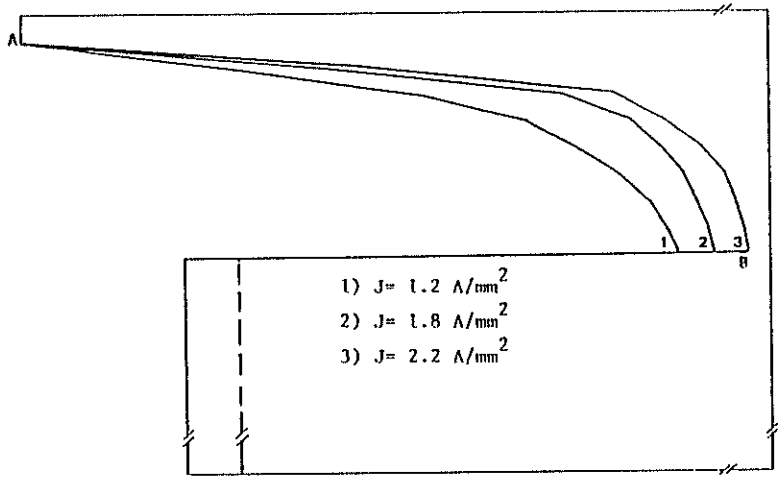

Fig. 6 -Polar surface shape for three different values of current density.

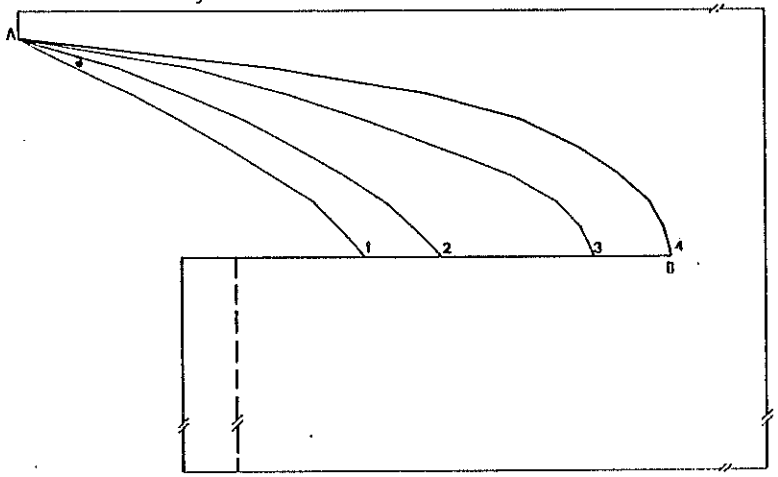

Fig. 7 -Polar surface shape at different iteration cycles:
1) initial profile
2) profile after three iteration cycles
3) profile after seven iteration cycles
4) profile after twelve iteration cycles;solution obtained with 0.3% accuracy.

4. ANALYSIS OF ERRORS

Concerning the accuracy with which the profiles may be obtained, the following causes, in addition to the inevitable truncation errors, are to be considered:

1) the errors relating to the numerical method used for the calculation potentials. This method envisages the change from a continuous system into a discrete system by means of finite elements that may be of a different order.
The error, therefore, is due to the nodal pitch in relation to the sizes of the domain, and will be thus different in the various zones as a function of the thickening made. Moreover, the pitch adopted being equal, the higher the order of the elements used, the lesser the error will be;

2) the errors made in the solution of the algebraic equations system at the finite elements using the Gauss-Seidl method. A calculation of this error may be made by comparing the maximum residue with the potential of the point where this maximum occurs;

3) the errors with which equations (7) and (8), supplying the coordinates of the profile points, are solved.
These equations are inserted into the iterative procedure described in paragraph 2., which, as it is interrupted after a finite number of iterations, involves the presence of a residue. Therefore, in order that the number of iterations to be performed may be established, it will be necessary to establish the maximum error with which we want to obtain the profile and, hence, the maximum possible residue. An estimate of this error may be made by calculating, on any iteration cycle, the percent difference between the values D_{ph} and D_{th} imposed by the project and the relative values calculated at the desired iteration.

With reference to the profiles of Fig. 7 obtained at a different number of iterations, the curve of the difference in percentage between the values of the imposed potentials and the calculated potentials, is shown in Fig. 8, as a function of the number of iterations. It may be observed that, as it appears from fig. 8, this error is not constant in the various points of the profile, and is greater in the points where the curve is more accentuated.
Furthermore, in the case under review, starting from the twelfth iteration the error may be regarded as negligible (0,3%) in relation to the geometrical dimensions of the considered system.
Still with reference to the determination of the final profile of fig. 7, the type-1) error is the one that is, percentagewise, the most important, elements of the first order having been used; the type-2) error, on the contrary, turns to be of non importance after a number of Gauss-Seidl iterations equal to 150.

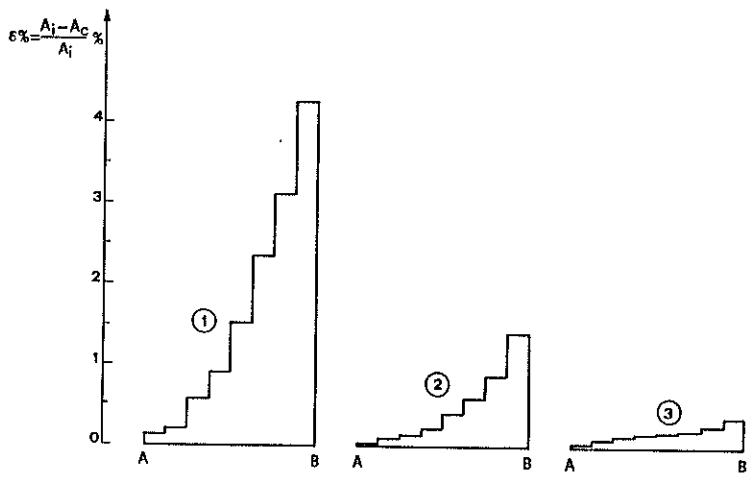

Fig. 8 - Difference (percent) between the values of the imposed potentials (A_i) and the calculated ones (A_c) along the polar surface:
1) at third iterations cycle
2) at seventh iterations cycle
3) at twelfth iterations cycle

Table II shows the values assumed by the three different errors for the case under examination:

TABLE II

type-1) error	3,4%
type-2) error	0,01%
type-3) error	0,3%

5. CONCLUSIONS AND FURTHER DEVELOPMENTS

The electrical and magnetic field analysis, carried out using numerical methods, may be profitably employed, not only for a better understanding of the functioning of electrical and magnetic equipment and machinery, but also for the purposes of their automatic planning in view of the obtainment of the pre-established performances.
In the present work an iterative procedure is set out that allows the automatic determination of electrical and magnetic profiles that verify some given project conditions.
The calculation methodology adopted, uses the finite element technique, that lends itself particularly well to the case under consideration, in which the boundary being unknown; it is necessary to approximate the physical system by means of a grid, also irregular, of discrete elements, whose nodes are not constrained to assume pre-established positions.
The proposed procedure is susceptible of further improvements and subsequent developments.
In the first place, it may be thought of improving the accuracy of the method by reducing some uncertainties already examined in the previous paragraph, arising out of the discretization of the continuous system with finite elements of the 1st order. The adoption of elements, whose order is higher than the first one, would allow to reduce such discretization errors, while at the same time obtaining a better accuracy and continuity in the calculation of the gradient vector.
In spite of the seeming complexity of the proposed procedure, the calculation program developed allows to come to a solution sufficiently accurate for the requirements of the practice in a few number of iterations, of the order of one tenth, provided that the boundary of the domain under examination is sufficiently regular.
In the case of more complex boundaries than the ones here considered, the convergence rapidity needs to be improved through the introduction of properly studied algorithms.
Finally, the calculation procedure set out here lends itself to being extended for the automatic determination of profiles in problems, in which project conditions are simultaneously imposed on both potential and field, as for instance, in the magnetic case, a problem for which both the conditions 1) and 2) of Table I will apply.

6. ACKNOWLEDGEMENT

The authors wish to express their most sincere gratitude to prof. Umberto Ratti for his valuable encouragement.

7. REFERENCES

1. O.C. Zienkiewicz, The finite element method in engineering science - McGraw-Hill, London, 1971
2. A. Di Napoli, C. Mazzetti, U. Ratti, A computerized program for the numerical solution of harmonic fields with boundary conditions non properly defined - Compumag, Oxford, May 1976.
3. M. Mele, Studio dei campi elettrici e magnetici con il metodo degli elementi finiti. Applicazione alla ricerca del profilo di un elettrodo in alta tensione. Tesi di laurea in Ingegneria elettrotecnica, Marzo 1978.

OPTIMUM DESIGN OF A MAGNET WITH LAGRANGIAN FINITE ELEMENTS

A. Marrocco - O. Pironneau
IRIA-LABORIA

I - INTRODUCTION

In this paper we shall discuss some aspects related to the design of systems for which a good numerical simulation by partial differential equations can be done. The typical situation is the following : some engineers and numerical analysts have spent a great deal of time at making an efficient numerical simulation of a system. This numerical scheme is now currently used by the engineers in the design of new products. There, the "know how" of the engineers is used : he knows that if such and such parameters are changed, such behaviour is induced. The numerical analyst raise the following question : can this be done automatically ? In general the answer is no ; indeed dialogues with engineers reveal that the criteria for optimal design are numerous and that the constraints are hundeeds.

However the numerical analyst can be of great help to the engineer's intuition. With respect to one differentiable criteria, he can

1 - give the optimum design under certain constraints

2 - tell the direction of changes to be done to improve design

The method proposed here operates in the physical plan and can be considered as a natural extension of the numerical study of the state equation. The method is the discrete analogue of the continuous case in O. PIRONNEAU [1] . The method is applied for the design of an electromagnet. The state equation is a non linear equation considered for example in R. GLOWINSKI - A. MARROCCO [2,] , [3] . (The classical magnetostatic equation in potential vector form). We have look for electromagnet with constant interpolar field but the technique can be adapted to other criteria and other P.D.E. The computation are done with triangular Lagrangian piecewise linear elements. The nodes are allowed to vary on pescribed curves (to avoid intercrossing, but it is not an obligation). The gradient of the criteria with respect to the coordinates of the moving nodes is computed analytically via an adjoint state equation and the criteria is then minimized by the method of steepest descent

II - STATEMENT OF THE MAGNETOSTATIC PROBLEM

We consider the classical magnetostatic equation in potential vector form

$$\nabla\times(\nu\times\vec{A}) = \mu_o\vec{J} \tag{2.1}$$

which can be in the two dimensional case written as

$$-\nabla.(\nu\nabla A_3) = \mu_o j_3 \tag{2.2}$$

or

$$\sum_{i=1}^{2}\frac{\partial}{\partial x_i}(\nu\frac{\partial A_3}{\partial x_i}) = \mu_o j_3 \tag{2.3}$$

In these previous equations μ_o is a constant equal to $4\pi\ 10^{-7}$ in MKSA system, ν the relative magnetic reluctivity, which is constant in air and cooper ($\nu = 1$) and is a non linear function of $|\vec{B}|^2 = |\nabla\times\vec{A}|^2 = |\nabla A_3|^2$ in the iron ($\vec{B}$ is the flux density vector)(see fig. 1, for an analytical approximation of the relative reluctivity ν by a function of the family

$$\tilde{\nu}_{\varepsilon,\alpha,C,T}(x) = \varepsilon+(C-\varepsilon)\frac{x^\alpha}{x^\alpha+T}$$

For the computation we take a bounded domain Ω, and the potential vector must satisfy suitable properties on the boundary of Ω. (see fig.2). On AD = Γ_1 we have natural symmetry condition , i.e. $\frac{\partial A_3}{\partial n} = 0$ (flux lines cross orthogonally this line), and on $\Gamma_o = \partial\Omega-\Gamma_1$ we have homogeneous Dirichlet condition (no flux lines cross this boundary Γ_o).

Let us define the functional space $\mathcal{V}$ by

$$\mathcal{V} = \left\{v, v\in L^2(\Omega), \frac{\partial v}{\partial x_i}\in L^2(\Omega), \quad v/_{\Gamma_o} = 0\right\} \tag{2.4}$$

It is easy to see that with the norm

$$v \longrightarrow \|v\|_{\mathcal{V}} = \int_\Omega|\nabla v|^2dx \tag{2.5}$$

$\mathcal{V}$ is an Hilbert space, and the magnetostatic problem can be formulated as an optimisation problem in the following way :

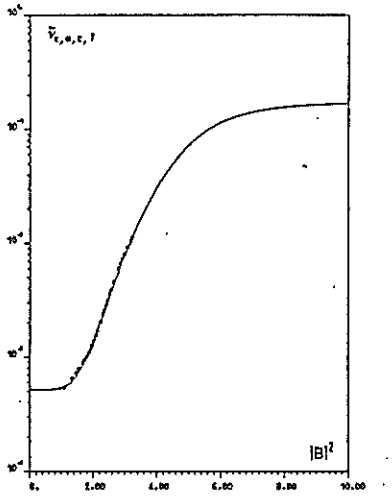

Analytical approximation of relative reluctivity $\bar{\nu}_{\epsilon,a,c,T}(|B|^2)$, ($\epsilon = 5.163619 \times 10^{-6}$, $a = 5.419241$, $c = 0.175775$, $T = 8.758756 \times 10^3$).

Fig. 1

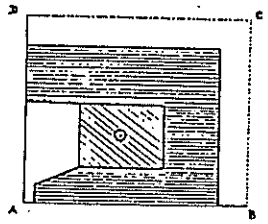

Computational domain.

Fig. 2

Find $A \in \mathcal{V}$ such that

(2.6) $\mathcal{J}(A) \leq \mathcal{J}(v)$ for every $v \in \mathcal{V}$

where $\mathcal{J}$ is given by

(2.7) $$\mathcal{J}(v) = \frac{1}{2}\int_\Omega \Psi(x, |\nabla v|^2)dx - \int_\Omega \mu_0 j v dx$$

with Ψ defined by

(2.8) $$\begin{cases} \dfrac{\partial \Psi}{\partial |\vec{B}|^2}(x, |\vec{B}|^2) = \nu(x, |\vec{B}|^2) \\ \Psi(x,0) = 0 \end{cases}$$

The optimization problem (2.6) has a unique solution (see R.GLOWINSKI - A. MARROCCO [2])characterized by the variationnal formulation

(2.9) $$\begin{cases} \displaystyle\int_\Omega \nu(x, |\nabla A|^2)\nabla A.\nabla v\, dx - \int_\Omega \mu_0 j v dx = 0 \qquad \forall v \in \mathcal{V} \\ A \in \mathcal{V} \end{cases}$$

For the finite element approximation the variational formulation (2.9) is used. The triangulation $\mathcal{T}_h^\circ$ will be a set of triangles T such that

(2.10) $$\bigcup_{T \in \mathcal{T}_h^\circ} T \subset \bar{\Omega}$$

For T_1 and $T_2 \in \mathcal{T}_h$ we have

(2.11) $$\begin{cases} T_1 \cap T_2 = \phi \\ \text{or } T_1 \text{ and } T_2 \text{ have a commom side} \\ \text{or } T_1 \text{ and } T_2 \text{ have common vertex} \end{cases}$$

(see for example fig. 3 for an initial triangulation)

The functional space $\mathcal{V}$ (2.4) is approximated by $\mathcal{V}_{oh}$

(2.12) $$\mathcal{V}_{oh} = \left\{ v_h \,|\, v_h \in \mathcal{C}^0(\bar{\Omega}_h), d^0 v_h \leq 1 \text{ on } T, T \in \mathcal{T}_h, v_h = 0 \text{ on } \Gamma_{oh} \right\}$$

where Γ_{oh} is the approximation of Γ_o
and we can express the approximated problem by

Find $A_h \in \mathcal{V}_{oh}$ such that

(2.13) $\mathcal{J}(A_h) \leq \mathcal{J}(v_h)$ for every $v_h \in \mathcal{V}_{oh}$

where $\mathcal{J}$ is given by (2.7)

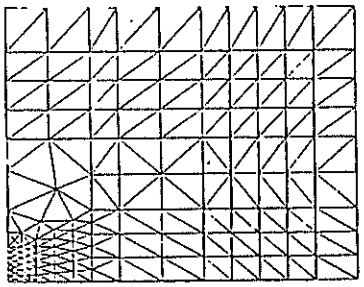

An initial triangulation (158 nodes, 267 elements).

Fig. 3

If $\omega_j(x), j = 1,2...N$ is a basis of the finite dimensional space $\mathcal{V}_{oh}$, the discrete potential vector can be expressed as

$$(2.14) \qquad A_h(x) = \sum_{i=1}^{N} A_i \omega_i(x)$$

and is solution of the variational non linear system

$$(2.15) \quad \begin{cases} \int_\Omega \nu(x,|\nabla A_h|^2)\nabla A_h.\nabla\omega_j \, dx - \int_\Omega \mu_0 j\omega_j \, dx = 0 \\ j = 1,2...N \end{cases}$$

II - STATEMENT OF THE OPTIMUM DESIGN PROBLEM (CONTINUOUS CASE).

Ω is an open set of R^n ($n = 2$ in our case), and j and E_d are two given functions of $L^2(\Omega)$. Let F be the ferrous region, C the copper region and $G = \Omega - \bar{F}\cup\bar{C}$

The potential vector A_F (which depends on the shape of ferrous region F), is solution of the non linear elliptic variational equality

$$(3.1) \quad \begin{cases} \int_\Omega \nu(x,|\nabla A_F|^2)\nabla A_F.\nabla\omega \, dx = \int_\Omega \mu_0 j\omega \, dx & \forall \omega \in \mathcal{V} \\ A_F \in \mathcal{V} \end{cases}$$

If D is some open subset of G, we wish to solve the problem

$$(3.2) \qquad \min_{F\in\mathfrak{F}} J(F)$$

where

$$(3.3) \qquad J(F) = \int_D |\nabla A_F - E_d|^2 dx$$

and $\mathfrak{F}$ is the set of admissible shapes for the ferrous region. For (3.2) to be well defined (with fixed copper region), we must have

$$(3.4) \qquad \mathfrak{F} = \left\{ F/F\subset\Omega, F\cap\Omega = \phi \right\}$$

Strictly speaking (3.2) is an optimal control problem for the distributed parameter system (3.1), where the control appears in the coefficient of the P.D.E. as a discontinuity of ν. Furthermore it should be pointed out that problem (3.2) is very similar to an optimum design problem (withNeumann condition on the unknown boundary).

Now let us outline how such problems can be solved by gradient techniques. More details can be found in O. PIRONNEAU [1].

Let F' be obtained from F by

$$(3.5) \qquad \partial F' = \left\{ x+\alpha(x) \quad | x\in\partial F \right\}$$

Where α is a given vector valued function (usually one takes $\vec{\alpha}(x) = \beta(x)\vec{n}(x)$, where $\vec{n}$ is the normal to ∂F).

We must be able to evaluate the first order term in α of the variation

$$\delta J = J(F') - J(F)$$

For the sake of clarity let us assume that D does not depend upon α from (3.3) with $\delta A_F = A_{F'} - A_F$

$$(3.6) \qquad \delta J = 2\int_D (\nabla A_F - E_d)\nabla\delta A_F dx + o(\delta A_F)$$

and from (3.1) with $\delta\nu = \nu(x,|\nabla A_{F'}|^2) - \nu(x,|\nabla A_F|^2)$

$$(3.7) \quad \begin{cases} \int_\Omega \left[\nu(x,|\nabla A_F|^2)\nabla\delta A_F.\nabla\omega + \delta\nu\nabla A_F.\nabla\omega \right] dx = o(\delta A_F) \\ \forall\, \omega\in\mathcal{V} \end{cases}$$

Now let us give the first order term for $\delta\nu$ evaluation

in $F'\cap F$ $\quad \delta\nu = 2\dot{\nu}(x,|\nabla A_F|^2)\nabla A_F.\nabla\delta A_F$

in $C'\cap C$ $\quad \delta\nu = 0$

in $F'\cap G$ $\quad \delta\nu = \nu(x,|\nabla A_{F'}|^2) - 1$

in $F\cap G'$ $\quad \delta\nu = 1 - \nu(x,|\nabla A_F|^2)$

Where $\dot{\nu}(x,|\nabla A|^2) = \dfrac{\partial}{\partial |\nabla A|^2}(\nu(x,|\nabla A|^2))$

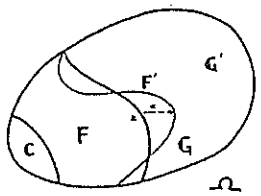

Ferrous regions F and F', copper region C, and complementary regions G and G'.

Fig.4

Therefore (3.7) becomes

$$(3.8)\quad \begin{cases} \int_\Omega \left[\nu(x,|\nabla A_F|^2)\nabla\delta A_F.\nabla\omega + 2\dot{\nu}(x,|\nabla A_F|^2)\nabla A_F.\nabla\delta A_F \nabla A_F.\nabla\omega\right]dx \\ +\int_{F'\cap G}\left[\nu(x,|\nabla A_{F'}|^2)-1\right]\nabla A_F.\nabla\omega dx \\ +\int_{F\cap G'}\left[1-\nu(x,|\nabla A_F|^2)\right]\nabla A_F.\nabla\omega dx = o(\delta A_F) \qquad \forall\,\omega\in\mathcal{V} \end{cases}$$

If $\alpha(x)<<1$ the last two integrals in (3.8) can be approximated by the surface integral

$$(3.9)\quad \int_{\partial F}\left[\nu(x,|\nabla A_F|^2)-1\right]\nabla A_F.\nabla\omega\vec{\alpha}(x).\vec{n}(x)ds \quad +o(\alpha)$$

Therefore if we define P_F as the solution in $\mathcal{V}$ of

$$(3.10)\quad \begin{cases} \int_\Omega\left[\nu(x,|\nabla A_F|^2)\nabla P_F.\nabla\omega+2\dot{\nu}(x,|\nabla A_F|^2)\nabla A_F.\nabla P_F\nabla A_F.\nabla\omega\right]dx = \\ 2\int_D(\nabla A_F-E_d).\nabla\omega dx \qquad \forall\,\omega\in\mathcal{V} \end{cases}$$

Then by letting $\omega=\delta A_F$ in (3.10) and $\omega=P_F$ in (3.8) we find from (3.6), (3.8), (3.9) that

$$(3.11)\quad \delta J=\int_{\partial F}(\nu(x,|\nabla A_F|^2)-1)\nabla A_F.\nabla P_F\vec{\alpha}(x).\vec{n}(x)ds \quad +o(\alpha)$$

Now it appears from (3.11) that by choosing $\alpha(x)$ such that

$$(3.12)\quad \vec{\alpha}(x).\vec{n}(x) = -\rho\,(\nu(x,|\nabla A_F|^2)-1)\nabla A_F.\nabla P_F\Big|_{\partial F}$$

(where ρ is a small positive parameter), we can decrease the criterion J by

$$(3.13)\quad \delta J = -\rho\int_{\partial F}\left[\nu(x,|\nabla A_F|^2)-1\right]^2\left[\nabla A_F.\nabla P_F\right]^2 ds$$

This is the essence of the gradient method :

0 - choose F_o, ρ and set $i=o$

1 - Compute A_{F_i}, P_{F_i} from (3.1), (3.10)

2 - Compute $\beta_i = -\left[\nu(x,|\nabla A_{F_i}|^2)-1\right]\nabla A_{F_i}.\nabla P_{F_i}\Big|_{\partial F_i}$

3 - Set $\partial F_{i+1} = \left\{x+\rho\beta_i(x)n(x)\,|\,x\in\partial F_i\right\}$

Set $i=i+1$ and go back to 1

IV - OPTIMUM DESIGN WITH FINITE ELEMENTS

The discrete vector potential $A_h=\sum_{i=1}^{N}A_i\omega_i$ is solution of

$$(4.1)\quad \int_\Omega\nu(x,|\nabla A_h|^2)\nabla A_h\nabla\omega_1 dx = \int_\Omega \nu_o j\omega_1 dx \qquad 1=1,2\ldots N$$

As is the continuous case we search for Ω such that ∇A_h is as close as possible to E_d in a subdomain D of Ω.

We define

$$(4.2)\quad J_h(\mathcal{T}_h) = \int_D |\nabla A_h - E_d|^2 dx$$

And we wish to find the coordinates of the nodes of $\mathcal{T}_h$ such that $J_h(\mathcal{T}_h)$ is minimum. Thus if χ is the set of admissible position of the nodes $X=\left\{x_k\right\}$, $k=1,2\ldots N$, then our problem is

$$(4.3)\quad \min_{X\in\chi} J_h(\mathcal{T}_h)$$

In order to apply a gradient method, we must compute

$$\partial_{\alpha_k} J_h(\mathcal{T}_h) = \lim_{\|\alpha_k\|\to o}(J_h(\mathcal{T}'_h)-J_h(\mathcal{T}_h))/\|\alpha_k\| \qquad (4.4)$$

for $k=1,2\ldots N$

Where $\mathcal{T}'_h$ is the triangulation obtained from $\mathcal{T}_h$ by moving the k^{th} node x_k into the position $x_k+\alpha_k$

It is convenient to assume that

$$(4.5)\quad D=\bigcup_{j\in J} T_j$$

Note that D may or may not depend upon α.

If E_d is piecewise constant on $\mathcal{C}_h$

$$(4.6)\qquad \delta J_h = J_h(\mathcal{C}'_h)-J_h(\mathcal{C}_h) = \sum_{j\in J}\left[\int_{T'_j}|\nabla A'_h-E_d|^2dx-\int_{T_j}|\nabla A_h-E_d|^2dx\right]$$

let be C and C' two sets of $\mathbb{R}^2$, we shall denote

$$(4.7)\qquad C\setminus C' = C-C'\cap C \qquad \text{(see fig.5)}$$

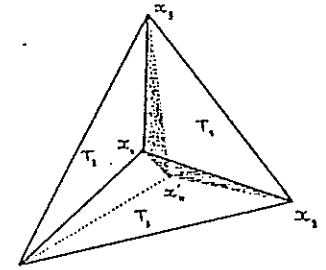

$T'_4\setminus T_4 = T'_4 - T_4\cap T'_4$

$T_4\setminus T'_4$

Transformation of the triangulation by moving the node x_k.

Fig.5

(4.6) can be written as

$$(4.8)\qquad \begin{aligned}\delta J_h = \sum_{j\in J}\Big[&\int_{T_j\cap T'_j}(|\nabla A'_h-E_d|^2-|\nabla A_h-E_d|^2)dx\\ &+\int_{T'_j\setminus T_j}|\nabla A'_h-E_d|^2dx-\int_{T_j\setminus T'_j}|\nabla A_h-E_d|^2dx\Big]\end{aligned}$$

If A_i is the value of the potential vector at node number i, let us introduce the following notations.

$$(4.9)\qquad \delta A_i = A'_i-A_i \qquad i = 1,2\ldots N$$

$$(4.10)\qquad \delta\omega_i(x) = \omega'_i(x)-\omega_i(x) \qquad i = 1,2\ldots N$$

Then

$$(4.11)\qquad \delta A_h = A'_h-A_h = \sum_{i=1}^{N}(A'_i\omega'_i-A_i\omega_i) = \sum_{i=1}^{N}(\delta A_i\omega_i+A_i\delta\omega_i+\delta A_i\delta\omega_i)$$

The KEY RELATION of the problem is

$$(4.12)\qquad \begin{cases}\delta\omega_i(x) = -\omega_k(x)\nabla\omega_i(x).\alpha_k + o(\alpha_k) & \forall\, x\in T_j\cap T'_j,\ \forall i,j \text{ such that } x_i \text{ and } x_k \text{ are nodes of } T_j\\ = o & \forall x\in T_j\cap T'_j,\ \forall i,j\ x_k\notin T_j\end{cases}$$

Therefore $\delta A_i\delta\omega_i$ is a higher order term, and the first integral of (4.8) is equal to

$$(4.13)\qquad 2\sum_{j\in J}\int_{T_j\cap T'_j}(\nabla A_h-E_d).\left[\sum_{i=1}^{N}\delta A_i\nabla\omega_i-\sum_{i\in I_{jk}}A_i(\nabla\omega_i\alpha_k)\nabla\omega_k\right]dx + o(\alpha_k)$$

where I_{jk} is the set of indices of nodes T_j if $x_k\in T_j$ and $I_{jk} = \emptyset$ if $x_k\notin T_j$.

Therefore if we let

$$(4.14)\qquad \tilde{\delta A} = \sum_{i=1}^{N}\delta A_i\omega_i$$

and denote by $\tilde{\alpha}_k(.)$ the function of $\left[L^2(\Omega)\right]^2$ such that

$$(4.15)\qquad \begin{cases}\tilde{\alpha}_k(x) = \alpha_k & \text{if } x \text{ and } x_k\in T_j\\ = o & \text{if } x\in T_j \text{ but } x_k\notin T_j\end{cases}$$

Then using the fact that the aera of domain $T'_j\setminus T_j$ and $T_j\setminus T'_j$ are of order α, (4.13) becomes

$$(4.16)\qquad \int_D 2(\nabla A_h-E_d)\left[\nabla\tilde{\delta A}-\nabla A_h.\tilde{\alpha}_k\nabla\omega_k\right]dx + o(\alpha_k)$$

It is easy to compute integral on $T'_j\setminus T_j$ and $T_j\setminus T'_j$ in (4.8) as boundaries integrals on the sides of T_j or T'_j, and by using Green's formula we can obtain

$$\int_D|\nabla A_h-E_d|^2\nabla\omega_k.\alpha_k dx + o(\alpha_k)$$

and finally (4.8) can be written

$$(4.17)\qquad \begin{aligned}\delta J_h = &\int_D 2(\nabla A_h-E_d)\left[\nabla\tilde{\delta A}-\nabla A_h.\tilde{\alpha}_k\nabla\omega_k\right]dx\\ &+\int_D|\nabla A_h-E_d|^2\nabla\omega_k.\alpha_k dx + o(\alpha_k)\end{aligned}$$

To evaluate the first term, we go back to (4.14), (4.9) and to the definition of A_i (2.14), and from equation (4.1) we have

$$(4.18)\quad \sum_j \int_{T'_j} \nu(x,|\nabla A'_h|^2)\nabla A'_h.\nabla\omega'_1 dx - \int_{T_j} \nu(x,|\nabla A_h|^2)\nabla A_h.\nabla\omega_1 dx = \int_\Omega \mu_o j.(\omega'_1-\omega_1)dx = o \qquad , 1 = 1,2...N$$

Using the same procedure in integral's evaluation we find that (more details can be found in [4])

$$(4.19)\quad \begin{cases} \int \left[\nu(x,|\nabla A_h|^2)\nabla\tilde{\delta A}.\nabla\omega_1 + 2\dot{\nu}(x,|\nabla A_h|^2)\nabla A_h.\nabla\tilde{\delta A}\nabla A_h.\nabla\omega_1\right] dx = \\ \int \left[\nu(x,|\nabla A_h|^2)\nabla A_h.\tilde{\alpha}_k\nabla\omega_k\nabla\omega_1 + 2\dot{\nu}(x,|\nabla A_h|^2)\nabla A_h.\nabla\omega_k\nabla A_h.\tilde{\alpha}_k\nabla A_h.\nabla\omega_1\right]dx \\ + \int_\Omega \nu(x,|\nabla A_h|^2)\left[\nabla A_h.\nabla\omega_k\nabla\omega_1.\tilde{\alpha}_k - \nabla A_h.\nabla\omega_1\nabla\omega_k.\tilde{\alpha}_k\right] dx \qquad +o(\alpha_k) \end{cases}$$

Then like in continuous case, by introducing the adjoint state $P_h \in \mathcal{V}_{oh}$ solution of

$$(4.20)\quad \begin{cases} \int_\Omega \left[\nu(x,|\nabla A_h|^2)\nabla\omega_1.\nabla P_h + 2\dot{\nu}(x,|\nabla A_h|^2)\nabla A_h.\nabla\omega_1\nabla A_h.\nabla P_h\right] dx \\ = \int_\Omega 2(\nabla A_h - E_d)\nabla\omega_1 dx \qquad 1 = 1,2...N \end{cases}$$

We obtain the following result :

Assuming that E_d is piecewise constant on $\mathcal{T}_h$ and that $j = o$ in T_j for all j such that $x_k \in T_j$, if $\mathcal{T}'_h$ is obtained from $\mathcal{T}_h$ by moving the k^{th} node from x_k to $x_k+\alpha_k$, then we have

$$(4.21)\quad \begin{aligned} J_h(\mathcal{T}'_h) - J_h(\mathcal{T}_h) = & \int_\Omega \nu\nabla A_h.\tilde{\alpha}_h\nabla\omega_k.\nabla P_h dx \\ & + \int_\Omega \nu\nabla A_h.\nabla\omega_k\nabla P_h.\tilde{\alpha}_k dx \\ & - \int_\Omega \nu\nabla A_h.\nabla P_h\nabla\omega_k.\tilde{\alpha}_k dx \\ & + \int_\Omega 2\dot{\nu}\nabla A_h.\nabla\omega_k\nabla A_h.\tilde{\alpha}_k\nabla A_h.\nabla P_h dx \\ & + \int_D |\nabla A_h - E_d|^2\nabla\omega_k.\tilde{\alpha}_k dx \\ & - \int_D 2(\nabla A_h - E_d).\nabla\omega_k\nabla A_h.\tilde{\alpha}_k dx \qquad +o(\alpha_k) \end{aligned}$$

It is easy to apply a gradient technique using (4.21)

V - NUMERICAL EXPERIMENTS

The numerical experiments have been made on the electromagnet showed in fig.2. The triangulation is composed of 267 triangles and 158 nodes. the number of unknows is 124.

We want to find the iron shape in the air gap in order to obtain a uniform distribution of the flux density in a subdomain D of this air gap. This region D can be fixed or can move with the iron boundary.

Let us give now the region of interest for the optimum design problem and show the parametrisation of the triangulation.

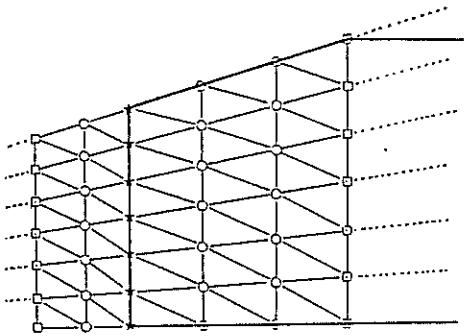

Triangulation of the region for an optimum design problem (o are fixed nodes, * are principal moving nodes, and o are associated moving nodes).

Fig. 6

- the nodes □ are fixed nodes
- the nodes * are the principal moving nodes (nodes at the boundary between iron an air), and the nodes o are associated moving nodes
- the coordinates of these associated moving nodes are simply related with coordinates of fixed nodes and principal moving nodes.
- all the "moving nodes" must move on pescribed curves (in our case straight lines).

See fig.7 for an admissible shape for the triangulation

5.1 - Numerical experiments with FIXED CRITERION DOMAIN

We can see in fig.8 the domain D where the criterion $J = \int_D |\nabla A_h - E_d|^2 dx$ is evaluated, and we can see also the initial iron geometry retained

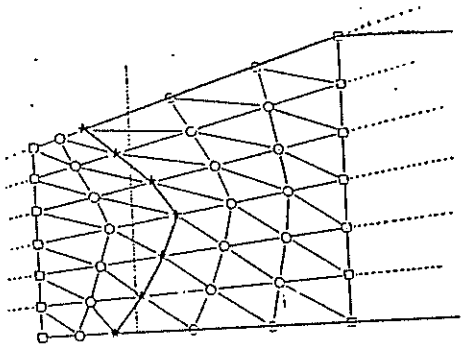

. Transformation of the triangulation by moving the nodes.

Fig.7

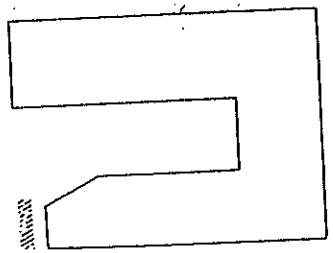

Initial geometry of the magnet with the fixed domain $\bar{D}\bar{C}\Omega$ where the criterion J is evaluated (examples 1, 2, 3).

Fig.8

EXAMPLE 1

The current density $j = 5 \times 10^6$ MKSA (even with this current density value the magnetostatic problem is non linear).

The parameter E_d in the criterion is

$E_d = (0,13)$ i.e. we want to have in D a uniform flux density $B = (1.3,0)$.

The starting value of the criterion is

$$J_o = 0.6116 \times 10^{-5}$$

and after 9 iterations in the optimization process (9 gradient steps) the criterion is

$$J_9 = 0.34\ 45 \times 10^{-5}$$

In figure 9 we can see the initial magnetostatic state and in fig.10 the magnetostatic state and air gap shape after optimization.

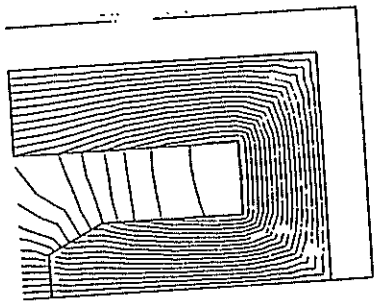

. Initial magnetostatic state (example 1).

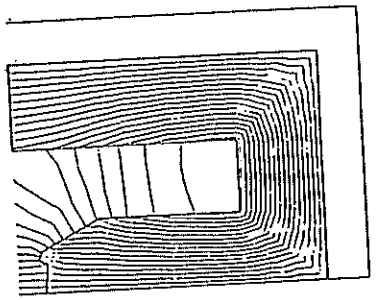

. Magnetostatic state and air-gap shape (example 1, step 9).

Fig.9

Fig. 10

EXAMPLE 2

- current density $j = 20 \times 10^6$ MKSA and

$E_d = (0,1.3)$

The initial value of the criterion is

$$J_o = 0.1003 \times 10^{-3}$$

and after 9 steps we obtain

$$J_9 = 0.4613 \times 10^{-6}$$

Note that at the first step the value is $J_1 = 0.6057 \times 10^{-6}$

In fig. 11 we give the initial magnetostatic state for $j = 20 \times 10^{-6}$ MKSA and in fig. 12 and 13 we give respectively the results at step 1 and 9 respectively

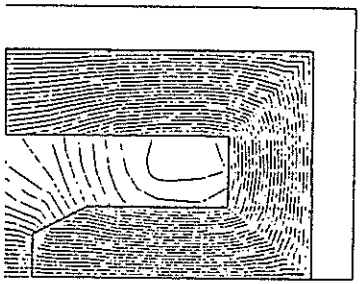

. Initial magnetostatic state (examples 2, 3, 4).

Fig.11

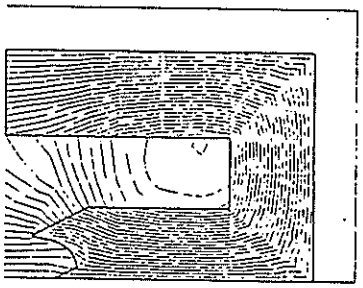

. Magnetostatic state and air-gap shape (example 2, step 1).

Fig.12

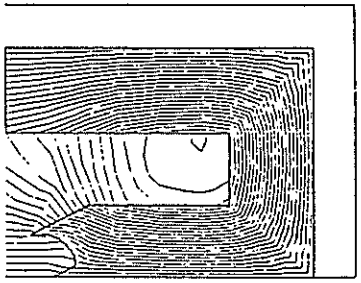

Magnetostatic state and air-gap shape (example 2, step 9).

Fig.13

We give in table 1 and 2 respectively the numerical value of flux density in the triangle lying in D for the initial state and after optimization.

Initial value of flux density B in the subset D (fixed)				Flux density B after optimization ($E_d = \{0, 1.3\}$)		
Triangle	Module	B_x	B_y	Module	B_x	B_y
240	1.60867	0.20220	1.59592	1.29559	0.09501	1.29210
241	1.64087	0.16562	1.63249	1.33829	0.04975	1.33736
242	1.60118	0.12910	1.59597	1.29213	0.00452	1.29213
243	1.56817	0.16568	1.55939	1.24786	0.04978	1.24687
244	1.80634	0.12910	1.80172	1.29889	0.00452	1.29889
245	1.86110	0.10560	1.85810	1.30013	0.00400	1.30012
246	1.80368	0.08216	1.80181	1.29891	0.00350	1.29891
247	1.74862	0.10566	1.74543	1.29768	0.00402	1.29768
248	1.86461	0.08216	1.86280	1.30322	0.00350	1.30322
249	1.90263	0.06595	1.90169	1.30800	0.00151	1.30800
250	1.86330	0.04969	1.86264	1.30316	−0.00051	1.30316
251	1.82495	0.06590	1.82376	1.29838	0.00149	1.29838
252	1.89919	0.04969	1.89855	1.30159	−0.00051	1.30159
253	1.92386	0.03931	1.92346	1.30337	−0.00125	1.30337
254	1.89842	0.02879	1.89820	1.30147	−0.00204	1.30147
255	1.87370	0.03917	1.87330	1.29969	−0.00130	1.29969
256	1.91882	0.02879	1.91861	1.29861	−0.00204	1.29861
257	1.93446	0.02224	1.93433	1.29745	−0.00156	1.29745
258	1.91842	0.01558	1.91836	1.29854	−0.00111	1.29854
259	1.90276	0.02213	1.90263	1.29970	−0.00159	1.29970
260	1.92936	0.01558	1.92930	1.29769	−0.00111	1.29769
261	1.93978	0.01123	1.93974	1.29662	−0.00066	1.29662
262	1.92918	0.00682	1.92916	1.29765	−0.00023	1.29765
263	1.91875	0.01117	1.91871	1.29872	−0.00068	1.29872
264	1.93397	0.00682	1.93396	1.29779	−0.00023	1.29780
265	1.94213	0.00342	1.94213	1.29751	−0.00011	1.29751
266	1.93394	0.00000	1.93394	1.29779	0.00000	1.29779
267	1.92577	0.00340	1.92577	1.29807	−0.00012	1.29807

$J = 0.46138507059 \times 10^{-6}$.

Table 1

Table 2

EXAMPLE 3

We take $j = 20 \times 10^{6}$ MKSA and

$$E_d = (0, 1.6)$$

The initial value of the criterion is

$$J_o = 0.2542 \times 10^{-4}$$

and after 8 gradient steps the value is

$$J_8 = 0.1886 \times 10^{-5}$$

the flux lines are plotted for step 1 and 8 in fig. 14, 15

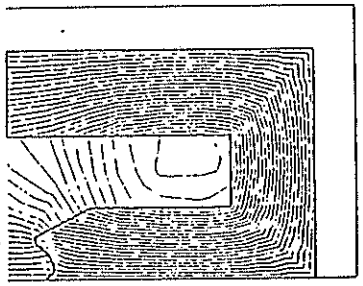

. Magnetostatic state and air-gap shape (example 3, step 1).

Fig. 14

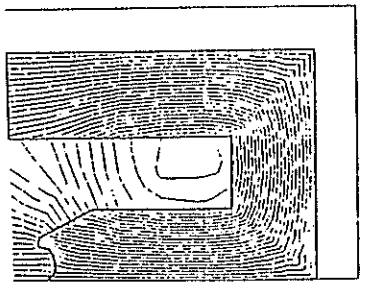

Magnetostatic state and air-gap shape (example 3, step 8).

Fig.15

5.2 - Numerical experiments with MOVING CRITERION DOMAIN

We can see in fig. 16 the initial domain D where the criterion J is evaluated . As the boundary between iron and air can move, the set D is a moving domain.

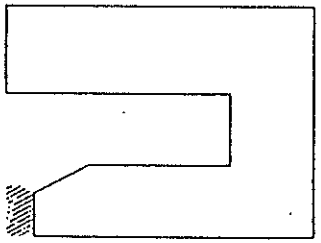

Initial geometry of the magnet with the variable domain $D \subset \Omega$ where the criterion J is evaluated (example 4).

Fig. 16

EXAMPLE 4

We take $j = 20 \times 10^{6}$ MKSA and

$$E_d = (0, 1.3).$$

The initial value of the criterion is

$$J_o = 0.2724 \times 10^{-3}$$

and we can reduce the value to

$$J_{56} = 0.6785 \times 10^{-6}$$

For this example the result is obtained with 3 runs in the following way. The first run is is made as in the previous examples. We perform 16 iterations and the final criterion value is

$$J_{16} = 0.1136 \times 10^{-4}$$

If we look at air-gap geometry, we observe an "oscillating " boundary (see fig.17) , for wich we substitue a straight boundary and obtain a new geometry (fig.18). The new value of the criterion after modification is

$$J_{16_*} = 0.9789 \times 10^{-5};$$

In the second run we perform 20 more iteration starting with this last initial state, and we obtain

$$J_{36} = 0.18465 \times 10^{-5}$$

We make a new manual fitting of the oscillating boundary and obtain a new geometry. The criterion value is then

$$J_{36_*} = 0.3607 \times 10^{-5}$$

In the third run we make 20 new iterations and obtain

$$J_{56} = 0.6785 \times 10^{-6}.$$

and the magnetostatic state is given in fig.19

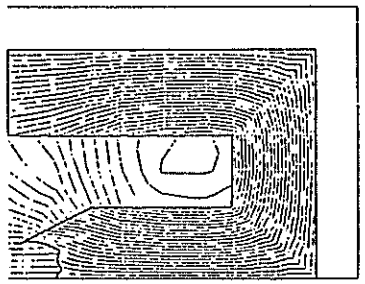

Magnetostatic state and air-gap shape (example 4, step 10).

Fig. 17

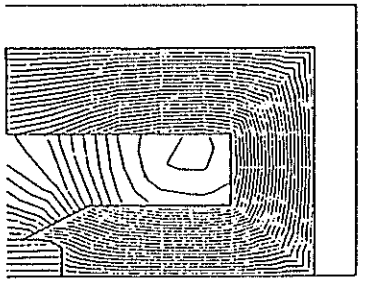

. Magnetostatic state and air-gap shape (example 4, step 16).

Fig.18

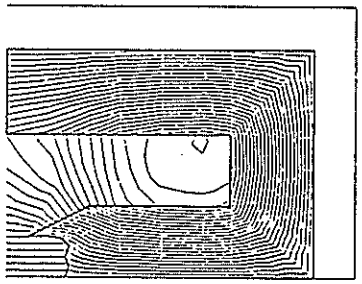

. Magnetostatic state and air-gap shape (example 4, step 56).

Fig. 19

EXAMPLE 5

The current density $j = 5 \times 10^6$ MKSA (initial magnetostatic state in fig.9), the domain D (criterion) is showed in fig. 20, and for $E_d = (0,0)$.

The initial value of the criterion is

$$J_o = 0.1384 \times 10^{-2}$$

and after 8 steps, the criterion value is

$$J_8 = 0.9747 \times 10^{-3}$$

and the magnetostatic state is given in fig. 21

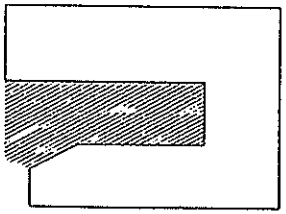

ZONE D EVALUATION DU CRITERE

Fig. 20

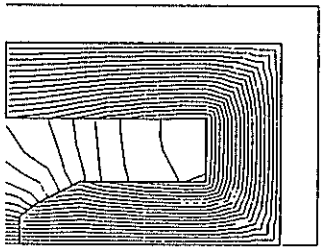

PAS ENTRE 2 LIGNES 0.
VALEURS EXTREMES DE LA FONCTION
0. 0.
DENSITE DE COURANT MKSA 0.
ETAT DESIRE B1= 0.
B2= 0.

Fig. 21

5.3 REMARKS

Thus, once the state equation is mastered, it takes only an additional "automatic" triangulation subroutine to optimize the design. However, it should be pointed out that the topology of the answer must be provided.

Let us also say that if the automatic triangulation subroutine is found to be too expensive to produce, one may compute the gradient vector only. Engineers find it to give very valuable information for the improvement of their design.

REFERENCES

[1] O. PIRONNEAU — Sur les problèmes d'optimisation de structure en mécanique des fluides- Thèse de Doctorat Paris VI. 1976

[2] R. GLOWINSKI-A. MARROCCO — Analyse numérique du champ magnétique d'un alternateur par éléments finis et surrelaxation ponctuelle non lineaire Computer methods in applied mechanics and engineering Vol3,n° 1, Janvier 1974

[3] R. GLOWINSKI-A. MARROCCO — Finite element approximation and itérative methods of solution for 2.D non linear magnetostatic problems. Proceeding of COMPUMAG conference Oxford1976, pp.112-125

[4] A. MARROCCO-O. PIRONNEAU — Optimum design with Lagrangian finite elements : design of an electromagnet . Rapport Laboria N° 251, Août 1977

CROSSTALK IN A PAM-TECHNIQUE TELEPHONE SWITCHING NETWORK DUE TO SKIN EFFECT APPROACH WITH THE FINITE ELEMENT METHOD

C. Lonati, G.C. Macchi and D. Raveglia
ITALTEL Società Italiana Telecomunicazioni, Milano, Italy

ABSTRACT

In the local telephone exchange of PROTEO switching system, signals from different sources are conveyed, in Time Division Multiplex (TDM) mode, into a transmission line (or bus) named "speech highway".

The speech highway crosstalk, which is dependent on the skin effect, is analyzed through the Finite Element Method (FEM).

FEM permits establishment of lumped-parameter equivalent circuits allowing the highway design to be optimized and provides a mathematical tool to study those phenomena which are generally estimated on an experimental basis only, since the analytical treatment is merely possible in special cases.

The possibility is provided to considerably reduce the crosstalk by introducing some ferrite elements in the speech highway. These ferrite elements should be properly placed so as to allow an efficient shaping of the magnetic field.

Very large network design is now possible using the proposed methods and the crosstalk is predictable.

1. INTRODUCTION

The crosstalk due to skin effect in the local telephone exchange of Proteo switching system is analyzed through the Finite Element Method.

Proteo is a fully-electronic integrated telecommunication system, which is likely to replace today's electromechanical and semi-electronic systems. It is capable of switching and transmitting voice, data and images. Essentially, it consists of three units: Central Control, Transit Network and Local Exchange.

The local exchange carries out the local user switching, directly, and routes the non-local traffic to the transit network. At present, several local exchanges are operating in Italy within the National Telephone Network.

Local exchange operates a Time Division Multiplex (TDM) switching with Pulse Amplitude Modulation (PAM). Connections between users are carried out through transmission lines, which are named "speech highways". Each speech highway permits 80 simultaneous connections, since it is assigned to 80 different pairs of users, in subsequent time slots (phases). Each time slot is lasting $125\,\mu s/80 = 1.56\,\mu s$, which enables to transmit, every second, 8000 conversation samples. Figure 1 illustrates two simultaneous pairs of connections using the same speech highway (hw).

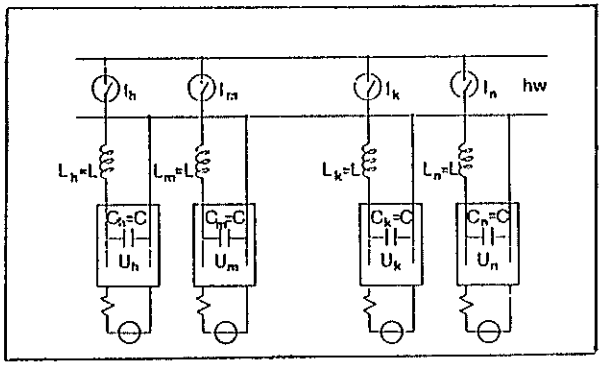

Fig. 1

In phase i, users U_h and U_k are connected by closing switches I_h and I_k for a time interval τ of about $1\,\mu s$.

Instead, in phase i+1, users U_m and U_n are connected by closing switches I_m and I_n.

During the following 78 phases, other 78 user pairs should be connected; at the end, connections start over again from phase 1.

In one ideal connection, during the time interval τ, lasting $\pi\sqrt{LC}$, a current pulse flows through speech highway, consisting of positive half-sinewave with an amplitude $(1/2)\sqrt{C/L}\,(V_h - V_k)$, where V_h and V_k are voltages on capacitors C_h and C_k, respectively, before switches I_h and I_k are closed.

In a non specific instant of τ, the current density is unequal in all points of a cross-section of each single speech highway conductor, because of the skin effect. When the switches I_h and I_k are open, the current flowing through the cross-section of the generic conductor is zero, but the current density is not zero in every cross-section points, because of previous current distribution non-uniformity. During the following time slot, a portion of the magnetic energy (associated with these eddy currents) flows into the user capacitors to which this phase was assigned, thus generating a crosstalk.

2. SKIN EFFECT EQUATION

Since, for long sections, speech highways are straight and with constant cross-sections, this problem may be handled as a two-dimensional case, namely by considering a plane perpendicular to the

highway axis. Besides, displacement currents can be neglected at the frequencies involved. Then the skin effect equation becomes as shown below:

$$\nabla^2 A - \mu g \frac{\partial A}{\partial t} = -\mu g E \qquad (1)$$

where A is the magnetic vector potential, E is the externally-applied electric field, μ is the magnetic permeability and g is the conductivity of the material. Knowing A, the current density J may be determined through the speech highway by using the following:

$$J = g \left(E - \frac{\partial A}{\partial t} \right) \qquad (2)$$

In our case, the field of integration of (1) has the form of fig. 2, where:

$$E(x,y,t) = \begin{cases} E_1(t) & \text{over } S_1 \\ E_2(t) & \text{over } S_2 \end{cases}$$

$$g(x,y) = \begin{cases} g_{cu} = 57.143 \times 10^6 \ \Omega^{-1} m^{-1} & \text{over } S_1 \cup S_2 \\ 0 & \text{over } S_o \end{cases}$$

$$\mu(x,y) = \mu_o \qquad \text{over } S_o \cup S_1 \cup S_2 \qquad (3)$$

with the Dirichlet boundary condition:

$$A\big|_\gamma = 0 \qquad (4)$$

S_1 and S_2 represent the cross-section of a speech highway, realized by a multilayer strip-line. S_o represents the dielectric.

As a matter of fact, the field of integration of the problem has a boundless extension since the radius tends to infinity.

In consequence of testing, R was selected about 5 times greater than the major geometrical dimension of the cross-section which is proper of the highway in order to prevent the distribution of the magnetic potential A from varying in conductor area, when R is increasing.

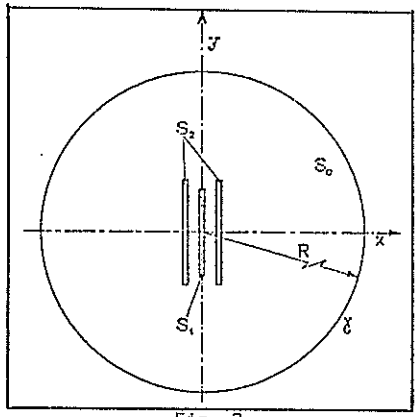

Fig. 2

In the practical case, equation (1) is difficult to integrate because of both material non-homogeneity and shape of the field of integration; an analytical solution may be found for very simple geometries only.

That's the reason for applying the Finite Element Method. Besides, the symmetry available would enable the study of one single quadrant in Fig. 2, provided Neumann condition was established:

$$\frac{\partial A}{\partial n} = 0$$

on axes X, Y.

3. ANALOGY WITH HEAT CONDUCTION EQUATION

3.a. SKIN EFFECT

An analogy exists between the skin effect and conduction heat propagation. This latter phenomenon is ruled by Fourier's equation which, in the case of isotropic material, is:

$$\lambda \nabla^2 \theta + q = c \rho \frac{\partial \theta}{\partial t} \qquad (5)$$

where θ is the temperature, q is the quantity of heat generated inside both time and volume unit, λ is the thermal conductivity, c is the specific heat of the material and ρ is the density of the material.

A similarity is thus established in variables involved in both the phenomena:

A	<-------->	θ	
E	<-------->	q	
$\mu_o g$	<-------->	$1/\lambda$	(in copper)
1	<-------->	$c\rho$	(in copper)
0	<-------->	$c\rho$	(in dielectric material)
g_f/g	<-------->	$c\rho$	(in ferromagnetic material)
$\mu_f \mu_o g$	<-------->	$1/\lambda$	(in ferromagnetic material)

This has enabled the analysis of the skin effect by using program FLHE (FLow of HEat), which employs the Finite Element Method to study the thermal conduction fields with various boundary conditions, in either transient or steady state.

FLHE is a component of a FEM program family realized by the CEGB, Berkeley Nuclear Laboratories, UK.

3.b. CAPACITANCE BETWEEN CONDUCTORS

FLHE is also used to calculate the capacitance between highway conductors. This capacitance evaluation is fundamental for both analysis and synthesis of the local exchange highway system.

Since electric potential V is described by Laplace's equation:

$$\nabla^2 V = 0, \tag{6}$$

the following analogy may be established with the heat propagation by conduction:

V	<-------->	θ
ε	<-------->	λ
E	<-------->	$\nabla\theta$

where ε is the dielectric permettivity and E is the electric field intensity.

At first, the distribution of electric potential V over the field S_o was calculated with FLHE, by imposing potential V = 1 and V = 0 to both conductors, respectively (Fig. 2).

Since teflon layers are placed between conductors, field S_o includes different materials.

From potential V, capacitance between conductors is calculated by evaluating the electrostatic energy W, using the following equation:

$$W = (1/2) \iint_{S_o} \varepsilon \, (\nabla V)^2 \, dx \, dy \tag{7}$$

Then, capacitance C is obtained from:

$$C = \frac{2W}{(V|_{S_2} - V|_{S_1})^2} \tag{8}$$

Integral (7) was calculated by means of a program, which operates the integration on each finite element taking the voltage values at the nodes, as obtained by FLHE, and then using quadratic shape functions and a 5-point Gauss integration formula.

3.c. GRAFIC OUTPUTS

Figures 3 and 4 illustrate the meshes used. They consist of isoparametric triangular and quadrilateral second-order elements.

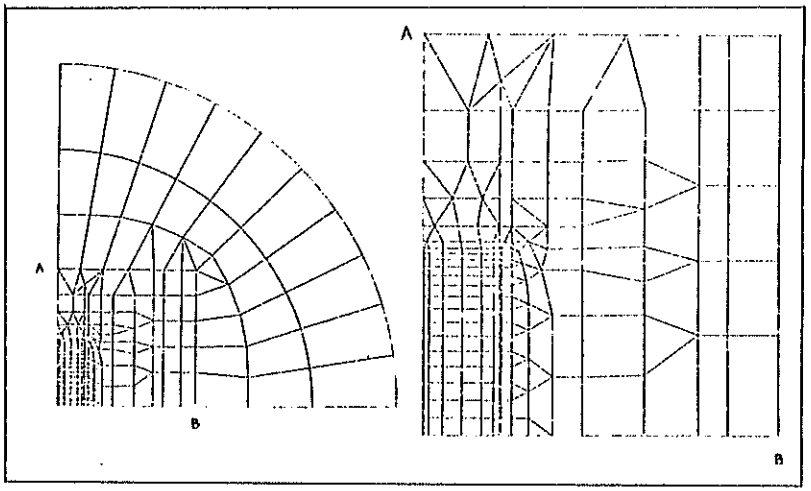

Fig. 3

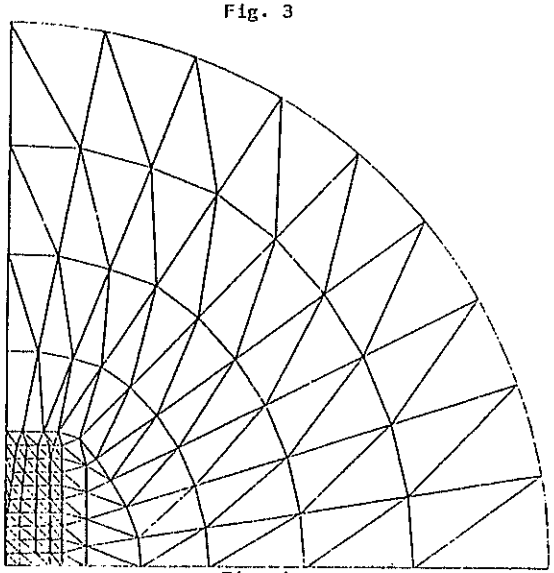

Fig. 4

Topological input data for FLHE were obtained by using a coordinatograph table and a program, realized specifically for this purpose, which can alter the mesh when the conductor dimensions are altered.

Figures 5 and 6 illustrate the equipotential curves of the electric field associated with the capacitance calculation program, with boundary conditions $V = 0$ and $(\partial V/\partial n) = 0$, respectively. The calculated capacitances are practically the same.

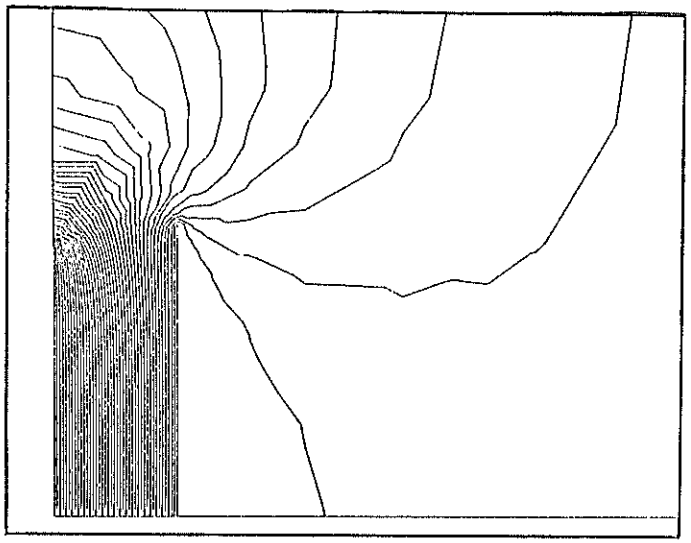

Fig. 5

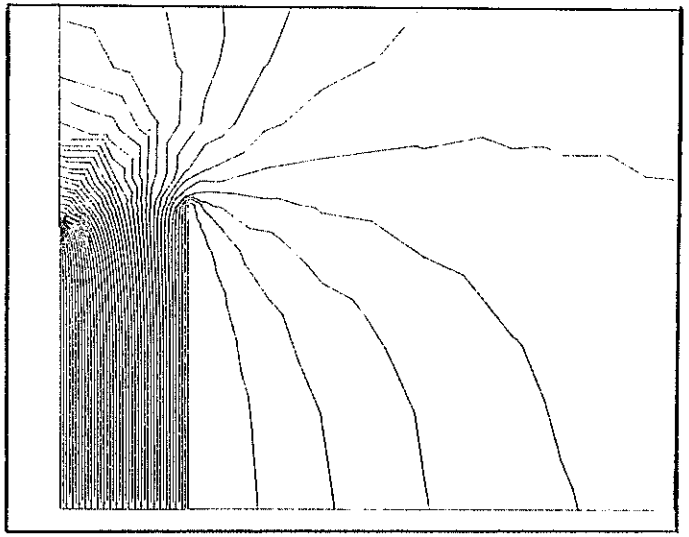

Fig. 6

Figure 7 is the plot of the magnetic vector potential when balanced dc currents are imposed (i.e., with reference to Fig. 2, current through S_1 is equal and opposite to current through S_2).

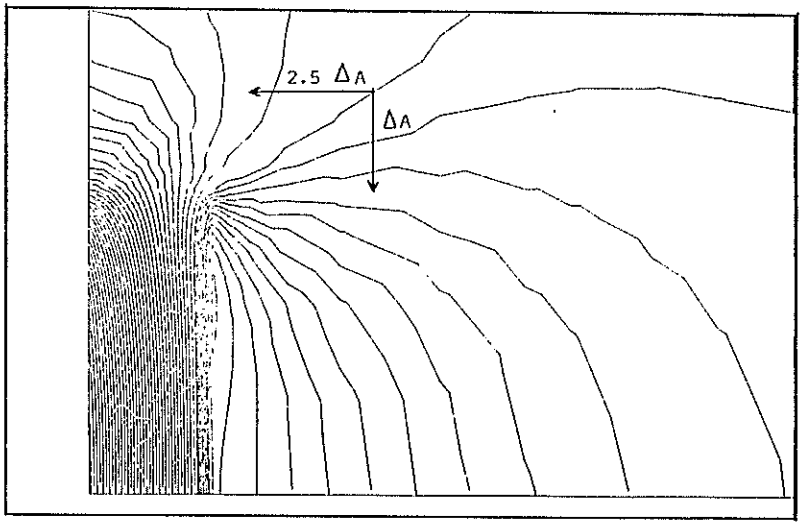

Fig. 7

4. LUMPED PARAMETER EQUIVALENT CIRCUIT OF SPEECH HIGHWAY

Figure 8 shows a lumped-parameter equivalent circuit of a short section Δl of the speech highway, which takes the skin effect into consideration.

During dead intervals, between consecutive TDM connections, some devices reset the electric field energy that was stored in the speech highway.

In our case, highway capacitance C_{hw}, calculated with the above-described method, has a negligible influence on the crosstalk calculation. This was verified through calculations carried out on models and experimental results.

Each branch of the equivalent circuit of Fig.8 corresponds to one, or more, of the finite elements into which conductors were divided.

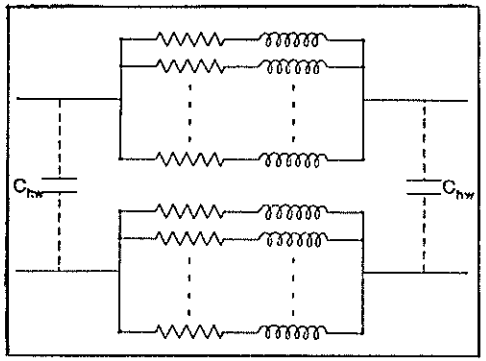

Fig. 8

Each branch consists of a resistance, a self-inductance as well as mutual-inductances with all others. Inductive parameters are obtained by dc-loading, one at a time, the finite elements forming the conductors.

Program FLHE provides the distribution of the magnetic vector potential A. The average value A_m on each element is obtained by using a quadratic interpolation starting from node values. These values enable the calculation of the inductive parameters. Comparison between the average value A_m on each element and that in the barycentre, and verification that mutual-inductances m_{ij} and m_{ji} are equal, (a necessary requirement for the reciprocity principle applied to pairs of elements, that were lumped in their respective barycentres) enable the evaluation of the quality of the discreteness and the validity of the equivalent circuit thus obtained.

The highest frequency in the validity range of this equivalent circuit is a function of both mesh fineness and number of equivalent circuit branches.

Current density in each finite element of conductors was supposed to be constant. This approximation validity was evaluated by calculating, using program ASTAP, the 2 MHz equivalent circuit response (2 MHz is the highest frequency of interest of this particular case).

This frequency response was compared with the results obtained by program TRIREPE, to which this same problem was submitted with a finer mesh with second-order elements. Deviation of results was less than 1%.

TRIREPE is a finite element program that CRIS-ENEL of Milan developed to study the thermal phenomena of dams in harmonic conditions.

ASTAP (Advanced STatistical Analysis Program) is a program developed by IBM to analyze electric networks under dc, ac and transient conditions, with either deterministic or statistical parameters.

The equivalent circuit, integrated with terminal circuit elements (Fig. 9), constitutes a time-division switching model with about 500 parameters.

Crosstalk was obtained by a transient analysis of this model accomplished by program ASTAP.

5. CROSSTALK CALCULATION BY CONVOLUTION INTEGRAL

The crosstalk calculation may be operated by the convolution integral whenever the highway response to Dirac's voltage pulse is known.

In thermal analogy, this is equivalent to evaluating the transient by imposing the following initial conditions: uniform temperature $\vartheta = 1$ on the pulse-strained conductor S_i ($i = 1,2$), and uniform temperature $\vartheta = 0$ on the remaining integrating field.

The transient response $A_1(x,y,t)$ to the voltage pulse yields the transient response $J_{ji}(x,y,t)$ of current density when the voltage step $u(t)$ is applied, because of the following relation:

$$J_{ji}(x,y,t) = g[u(t) - A_1(x,y,t)] \qquad (9)$$

The crosstalk of the circuit, with sequence operating switches, shown in Fig. 9, may be evaluated by considering the time-invariant circuits corresponding to the following situations: closed switches and open switches.

Figure 10 illustrates the invariant circuit that is valid in the first transient phase; the highway is represented by the two-port with terminals 1-2, 3-4, and is featured by currents $I_{ji}(t)$ ($i = 1,2$; $j = 1,2$), where $I_{ji}(t)$ is the current flowing along the speech highway conductor i, when a step voltage is applied across the terminals of conductor j, while the other conductor terminals are short-circuited. $I_{ji}(t)$ are calculated through a suitable program, starting from two transient analysis obtained by FLHE.

The equations below refer to the analysis of the circuit illustrated in Fig. 10.

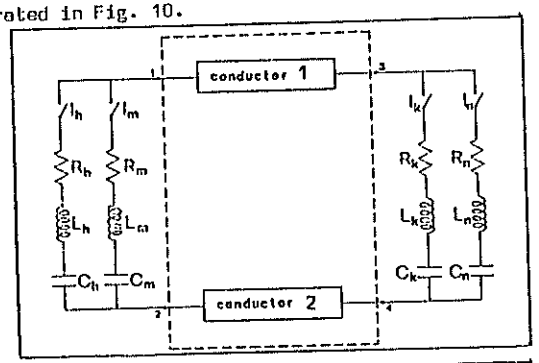

Fig. 9

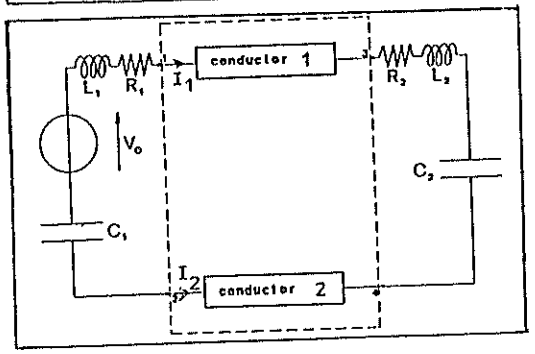

Fig. 10

$$\int_0^{t+\Delta t} I_1(\tau)\,d\tau = \int_0^{t+\Delta t} I_{1\Gamma 1}(t+\Delta t-\tau)\,V_{13}(\tau)\,d\tau + \int_0^{t+\Delta t} I_{2\Gamma 1}(t+\Delta t-\tau)\,V_{24}(\tau)\,d\tau \qquad (10)$$

$$\int_0^{t+\Delta t} I_2(\tau)\,d\tau = \int_0^{t+\Delta t} I_{1\Gamma 2}(t+\Delta t-\tau)\,V_{13}(\tau)\,d\tau + \int_0^{t+\Delta t} I_{2\Gamma 1}(t+\Delta t-\tau)\,V_{24}(\tau)\,d\tau \qquad (11)$$

$$V_{12}(t) = V_0 - \frac{1}{C_1}\int_0^t I_1(\tau)\,d\tau - L_1\frac{dI_1(t)}{dt} - R_1 I_1(t) \qquad (12)$$

$$V_{34}(t) = \frac{1}{C_2}\int_0^t I_1(\tau)\,d\tau + L_2\frac{dI_1(t)}{dt} + R_2 I_1(t) \qquad (13)$$

$$V_{12}(t) - V_{13}(t) - V_{34}(t) + V_{24}(t) = 0 \qquad (14)$$

$$I_1(t) = -I_2(t) \qquad (15)$$

These equations were integrated with the finite difference method, by considering $I_1(t+\Delta t)$, $I_2(t+\Delta t)$, $V_{12}(t)$, $V_{13}(t)$, $V_{34}(t)$, $V_{24}(t)$, as unknown quantities; besides, these equations provided the initial conditions for the invariant circuit, which is valid in the second transient phase.

The use of the convolution integral avoids the calculation of the numerous parameters of the equivalent circuit of Fig. 8 and gives more accurate results because it is not necessary to consider constant current density in each finite element of the conductors.

On the other hand, the equivalent circuit approach offers advantages in the highway synthesis because, by utilizing a proper mesh, the geometrical conductor variation (obtainable by either activating or deactivating some finite elements), corresponds to either an addition or deletion of branches to and from the equivalent circuit.

6. MAGNETIC FIELD SHAPING BY INTRODUCTION OF FERRITE ELEMENTS

The possibility is provided to considerably reduce the crosstalk by introducing some ferrite elements in speech highways. These ferrite elements should be properly placed so as to allow an efficient shaping of the magnetic field.

A non-uniform current distribution over a speech highway conductor cross-section is causing crosstalk in the TDM transmission.

Usage of thin conductors (+) provides a possibility of reducing such a non-uniformity in the thickness direction; in the direction perpendicular to the tickness the irregularity disappears when the cross-section has a radial symmetry.

Hence, the good behaviour versus the crosstalk of a coaxial speech highway having thin ring cross-section conductors.

In practice, teflon is used as a dielectric in order to minimize the dielectric hysteresis phenomena. Besides, the availability of a plane structure with laminated conductors, results to be an useful solution, because a coaxial teflon structure has a difficult technological embodiment. On the other hand, even an indefinite flat line with three thin conductors (Fig. 11), which is obtainable by extending the radii of the three conductors of a coaxial line, such as that specified in Fig. 12, to infinity, shows favourable crosstalk characteristics.

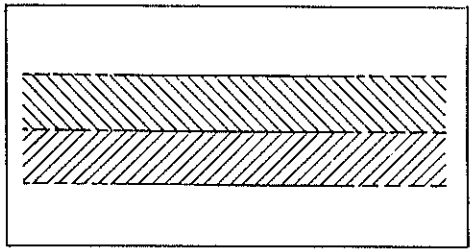

Fig. 11

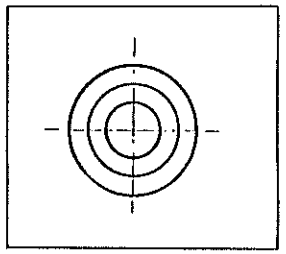

Fig. 12

Passing from this ideal structure to a realizable one (Fig. 13), which consists of three conductors having a finite width (such as those we examined so far), the magnetic field would be unchanged within the line if appropriate boundary conditions are imposed on margins A-A and B-B. This is possible by bringing the structure, in A-A and B-B, into contact with a material having a high and constant initial magnetic permeability in our interesting frequencies.

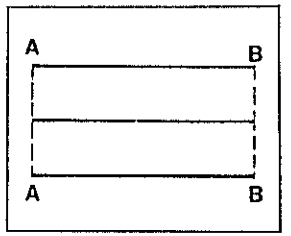

Fig. 13

A practical realization is possible by placing ferrite elements as shown in Fig. 14.

The structure with ferrite elements was analyzed by the above methods by using the mesh illustrated in Fig. 15, where the ferrite is symbolized by the shaded area.

The low values of magnetic field intensity make it possible to linearize the ferrite magnetization curve in the working area.

The remarkable improvement thus obtained is noticeable by comparing Fig. 7, relative to a ferriteless structure and Fig. 16, re-

---

(+) By thin conductors we mean those conductors having a lower thickness than depth of penetration $\delta = \sqrt{\rho/\pi f \mu}$, where ρ is the resistivity of the material, μ is its permeability and f is the frequency.

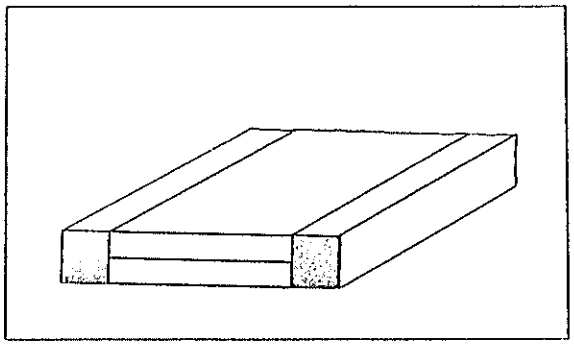

Fig. 14

lative to a structure comprising ferrite with μ_i = 1000, which refer to equal loading conditions. These figures illustrate the equipotential lines of A (which is everywhere perpendicular to the surface of the drawing), in the case of conductors loaded with balanced dc currents.

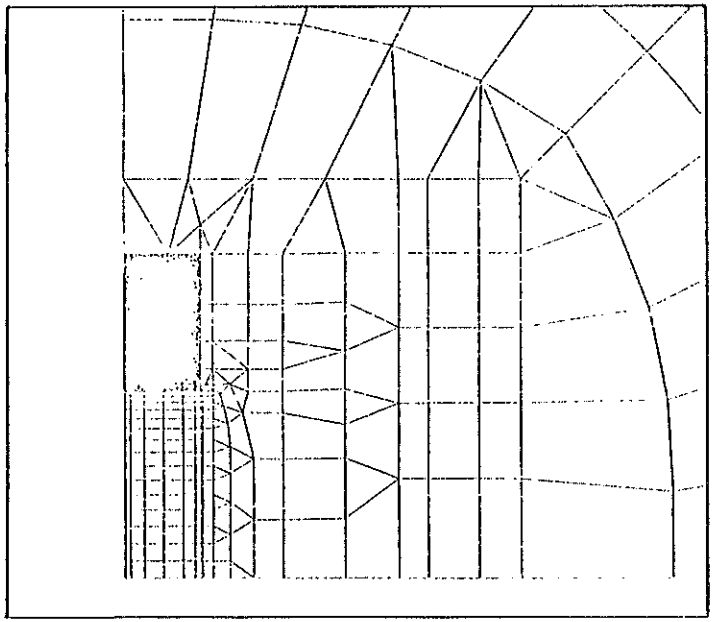

Fig. 15

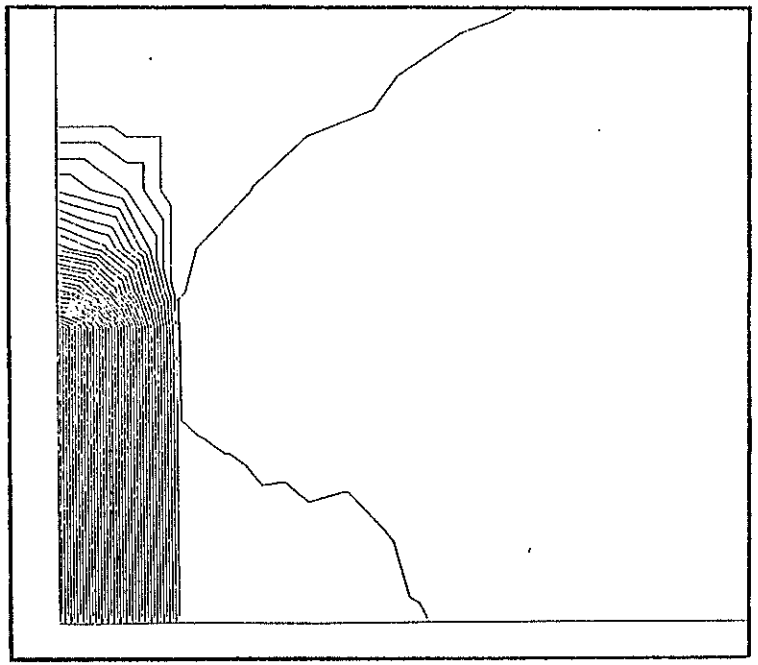

Fig. 16

7. CONCLUSIONS

The experimental tests of crosstalk due to skin effect confirmed the values obtained by digital simulation; these tests are difficult to carry out when crosstalk values are small (about -90 dB per meter of highway).

In the case of ferriteless highways, experimental tests and calculation results gave dB crosstalk values with a 1.2% deviation.

In the case of highways with ferrite elements, very small crosstalk values (about -135 dB) were obtained from the digital simulation; only one qualitative confirmation was obtained by experimental measurements.

Methodologies developed enable the design of conductors for each single switching network branch, by foreseeing performances in advance to its physical realisation; often, this is time consuming and expensive. Besides, it is possible to delve into crosstalk phenomena caused by eddy currents in local exchange transmission paths and to simulate very large switching networks, by also considering other crosstalk causes and real working conditions.

REFERENCES

1. D. Raveglia, A. Vicentini, "Centrale Terminale Proteo: alcuni aspetti teorici e funzionali delle caratteristiche di trasmissione", Telecomunicazioni, n. 54-55, marzo-giugno 1975.

2. L. A. Pipes, "Applied mathematics for engineers and physicists", McGraw-Hill, 1958.

3. O. C. Zienkiewicz, Y. K. Cheung, "Finite elements in the solution of field problems", The Engineer, n. 220, 1965, pp. 507-510.

4. M. Fanelli, "Il metodo degli Elementi Finiti: possibilità di applicazione a problemi di interesse degli elettrotecnici", L'Elettrotecnica, n. 6, giugno 1975.

5. A. Di Monaco, G. Giuseppetti, G. Tontini, "Studio dei campi elettrici e magnetici stazionari con il metodo degli Elementi Finiti", L'Elettrotecnica, N. 7, luglio 1975.

6. E. L. Wilson, R. E. Nickell, "Application of the Finite Element Method to heat conduction analysis", Nuclear engineering and design, vol. 4, 1966, pp. 276-286.

7. O. W. Andersen, "Laplacian electrostatic field calculation by finite elements with automatic grid generation", IEEE Trans. PAS, n. 92, 1973, pp. 1485-1492.

8. A. Konrad, J. L. Coulomb, J. C. Sabonnadière, P. P. Silvester, "Eigenvalue analysis of steady-state skin effect", ICCAD Int. Conf. on Num. Meth. in Electr. and Magn. Field Problems - Santa Margherita (I), 1976.

9. M. V. K. Chari, "Finite element solution of the eddy current problem in magnetic structures", IEEE Trans. PAS, n. 93, 1974.

10. J. Donea, S. Giuliani, A. Philippe, "Finite elements in the solution of electromagnetic induction problems", Int. Journal for Numer. Methods in Engin., vol. 8, 1974, pp. 359-367.

11. C. J. Carpenter, "Finite element network models and their application to eddy current problems", proc. IEE, vol. 122, n. 4, 1975.

12. T. K. Hellen, S. J. Protheroe, "The BERSAFE finite element system", Computer Aided Design, vol. 6, n. 1, january 1974.

APPLICATION OF THE PENALITY FUNCTION TO THE OPTIMIZATION OF THE MAGNETIZATION PROCESS

S. K. Krzemiński

Institute of the Theory of Electrical Engineering and Electrical Measurements
Technical University, Koszykowa 75, 00-661 Warsaw
POLAND

ABSTRACT

In the paper has been represented application of the penalty function methods to the problem of determination of the optimum distribution and course of magnetic induction on the edge of an elliptic magnetic cylinder so as to obtain, after predetermined time, distribution of induction assigned to the cylinder cross-section. For the inquired distribution has been defined the quality criterion in the form of the functional of mean quadratic error complemented by components of penalty which take into account limitations imposed on the searched function. The obtained modified quality funotional has been brought by method of Lagrange approximation by means of the second order finite element to the quadratic form optimization.

1. INTRODUCTION

R. Courant has introduced for the first time the role of the penalty function to variation problems. [7] L. Lions has it proposed to optimization of evolution problems in the work [6]. A widened mathematical ustification for this method gare A.V.Balakrishnan [2]. Actually this method is applied to problems of synthesis, identification and optimization of systems with distributed parameters. Its mathematical substance is following: the problem of searching the extreme of a functional with limitations is reduced to the problem of determination of the extreme without himiltations, which makes an easier problem. In this work this method has been applied to determination of Neumanian boundary conditions $\partial A/\partial n$ belonging to the space of admissible magnetization U_{ad} determined on the edge $\Sigma = \Gamma \times (0,T)$ of a magnetic cylinder of cross -section $\Omega \subset R^2$ and edge Γ, for vector potential $A(x,t)$ belonging to the space of state $L^2\{0,T,H^1(\Omega)\}$ [1, 6], satysfing in the region $Q = \Omega \times (0,T)$ the state oquation, as well as initial and boundary conditions. The state equation jojnitly with initial and boundary conditions compose limitations for the extreme of quality functional, $J(A,b)$. By introducing penalty functionals 2,6 these limitations have been added to the quality functional, thus forming a new $J(A,b)$. This proof of existance and univocal character of the extremo of modified functional presented J.L.Lions [6]. To construction of the optimum couple $\{A_\varepsilon, b_\varepsilon\}$ has been aplied approximation of the state function $A(x,t)$ and boundary magnetization $b(x,t)$ by means of the second order finite space element [8]. In consequence of the accepted approximation the stated problem has been reduced to optimization of quadratic form with respect the state vector $\{A\}$ and boundary magnetization vector $\{b\}$ in a finitely dimensional space.

2. STATEMENT OF OPTIMUM MAGNETIZATION PROBLEM

The electrodynamical state on the crossq-section of the cylinder is described by the Maxwell s equations set [6]

$$\text{rot } \mathbb{H} = \mathbb{j} \quad , \tag{2.1}$$

$$\text{rot } \mathbb{E} = -\frac{\partial \mathbb{B}}{\partial t} \quad , \tag{2.2}$$

$$\text{div } \mathbb{B} = 0 \; ; \quad \text{div } \mathbb{D} = 0 \; . \tag{2.3}$$

Introducing electrodynamic vectorial potential $A(x,t)$ by relation

$$\text{rot } A(x,t) = \mathbb{B}(x,t) \quad , \tag{2.4}$$

the above set has been substituted by one equation of parabolic type, for which will bo stated the problem of optimum boundary magnetization.
The electrodynamic vectorial potential $A(x,t) \in L^2\{0,T; H^1(\Omega)\}$ in the region $Q = \Omega \times (0,T)$ satisfies the state equation

$$\left\{ \frac{\partial A}{\partial t}(x,t,b) + \mathcal{L} A(x,t,b) = 0, \quad (x,t) \in Q \right. \tag{2.5}$$

as well as boundary and initial conditions

$$\frac{\partial A}{\partial n} = b(x,t) \; ; \quad (x,t) \in \Sigma \; , \tag{2.6}$$

$$A(x,0,b) = A_0(x), \; x \in \Omega \; , \tag{2.7}$$

where $\mathcal{L}$ is elliptic operator

$$\mathcal{L}(A) = \sum_{i=1}^{2} \frac{\partial}{\partial x_i} \left(\frac{1}{\mu_{ij}} \frac{\partial A}{\partial x_i} \right) \; , \tag{2.8}$$

$b \in L^2(\Sigma)$, $A_0 \in L^2(\Omega)$ are spaces of functions integrable with square and $H^1(\Omega) = \{ A : A \in L^2(\Omega); \frac{\partial A}{\partial x_i} \in L^2(\Omega) \}$ is the Sobolev space [1, 6].

We hare to determine function $b(x,t)$ which:

1. belongs to space of admissible boundary magnetizations $U_{ad} \subset U$

$$U_{ad} = \{ b; \quad b \in L^2(\Sigma), \quad \Sigma = \Gamma \times 0,T \}, \qquad (2.9)$$

2. after time $T < \infty$ will create the magnetic state of the conductor

$$A_d(x) \in L^2(\Omega) \; ; \; \Omega \in R^2 \quad ,$$

3. together with generalized solution $A(x,t)$ of the problem (2.5) + (2.7) will satisfy condution

$$J(b) = \inf J(v) \quad , \qquad (2.10)$$

$$v \in U_{ad}$$

where

$$J(b) = \int_{\Omega} (A(x,T) - A_d(x))^2 \, dx + \gamma \int_{\Sigma} b^2(x,t) dx dt, \qquad (2.11)$$

is the quality functional of the stated problem, γ is a number over zero.

Theorem 1: When the set of admissible magnetizations U_{ad} is closed and convex and the bilinear form $a(t,a,v)$

$$a(t,A,v) = \int_{\Omega} \sum_{ij} \frac{1}{\mu_{ij}} \frac{\partial A(x)}{\partial x_j} \frac{\partial v}{\partial x_i} dx \, , \qquad (2.12)$$

induced by the operator $\mathcal{L}(A)$, (2.8),

i) for each couple A, $v \in L^2\{0,T,H^1(\Omega)\}$ is measurable function versus variable t for $t \in (0,T)$;

ii) for each A and t belonging to $\in L^2\{0,T,H^1(\Omega)\}$ this form satisfies condition of coercivity

$$a(t,A,A) \geqslant \alpha \|A\|^2_{L^2(\Omega)} \, , \quad \alpha > 0 \qquad (2.13)$$

then the optimum magnetization $b(y,x,t) \in U_{ad}$ does exist and necessary and sufficient condition of its optimality is fulfilment of the following conditions

iii)

$$\gamma \frac{\partial \tilde{A}}{\partial t} + \mathcal{L} \tilde{A} = 0 \quad \text{in} \quad Q \, , \qquad (2.14)$$

$$\frac{\partial \tilde{A}}{\partial n} = \tilde{b} \quad \text{on} \quad , \qquad (2.15)$$

$$\tilde{A}(x,0) = A_0(x) \quad \text{in} \quad , \qquad (2.16)$$

$$-\frac{\partial p}{\partial t} + \mathcal{L}^* p = 0 \quad \text{on} \quad Q \, , \qquad (2.17)$$

$$\frac{\partial p}{\partial n} = 0 \quad \text{on} \quad , \qquad (2.18)$$

$$\int_{\Sigma} (p + \gamma \tilde{b})(b - \tilde{b}) dx dt \geqslant 0 \quad , \quad b \in U_{ad} \qquad (2.19)$$

where $(\tilde{A}, \tilde{b})$ is a couple of optimum distributions in Q and on the edge Σ, $p(x,t)$ is the state function conjugate with state $A(x,t)$, conjugate variable, and is expressed by relation

$$p(x,T) = \tilde{A}(x,T) - A_d(x), \quad x \in \Omega \qquad (2.20)$$

$\mathcal{L}^*(A)$ is eliptic operator conjugate with operator $\mathcal{L}(A)$ (2.8)

$$\mathcal{L}^*(A) = - \sum_{i,j=1}^{2} \frac{\partial A}{\partial x_j} \left(\frac{1}{\mu_{ij}} \frac{\partial A}{\partial x_i} \right). \qquad (2.21)$$

Condition (2.19) is a generalized form of principle of Pontriagin maximum.

Determination of the optimum magnetizing $\tilde{b}$ analytically from optimality conditions (2.14) + (2.19) with respect to quality criterion is connected with considerable difficulties and is feasible in particular cases. In work [5] basic limitation which is expressed by the generalized state equation has been taken into account at optimization of quality functional by numerical determination of the operator repesenting the source function as state function. This procedure leads to considerable expenditure of calculation. Hence, it is worth while to apply other methods. The most universal is here the method of penalty function [2, 6].

3. THE METHOD OF PENALTY FUNCTION

General methodics of penalty functionals consist in such modification of the quality functional (2.11) only to obtain the problem without limitations, equivalent or convergent in some sense to the preliminary problem with limitations [2, 6]. The problem stated in the preceding paragraph, i.e. optimization problem of boundary magnetization $b(x,t)$ with final observation $A(x,T)$.

(2.10) has principal, main limitations in the form of state equation (2.5) as well as boundary (2.6) and initial conditions which, according to essence of the method, will be added to the functional (2.11). In consequence we will obtain the modified functional of two variables, i.e. the state function $A(x,t)$ and boundary magnetization $b(x,t)$.
By introducing a new set of functions

$$Y = \{A;\ A \in L^2(0,T;\ H^1(\Omega)),\ \frac{\partial A}{\partial t} + \mathcal{L}A \in L^2(Q)\ ,$$

$$\frac{\partial A}{\partial n} \in L^2(\Sigma)\ \} \qquad (3.1)$$

and assuming penalty factor

$$\varepsilon = \{\varepsilon_1\ \varepsilon_2\ \varepsilon_3\};\quad \varepsilon_i > 0\quad i=1,2,3 \qquad (3.2)$$

in the space (Y,U) we determine the modified quality functional

$$J_\varepsilon(A\ b) = J(b) + \frac{1}{2\varepsilon_1}\ \left\| \frac{\partial A}{\partial t} + \mathcal{L}A \right\|^2_{L^2(Q)} +$$

$$+ \frac{1}{2\varepsilon_2}\ \left\| \frac{\partial A}{\partial n} - b \right\|^2_{L^2(\Sigma)} + \frac{1}{2\varepsilon_3}\ \left\| A(x,0) - A_0(x) \right\|^2_{L^2(\Omega)} \qquad (3.3)$$

where norms in space $L^2(Q)$ and $L^2(\Sigma)$ are expressed by relations

$$\|A(x,t)\|_{L^2(Q)} = \left\{ \int_0^T |A(x,t)|^2\ dxdt \right\}^{\frac{1}{2}} \qquad (3.4)$$

$$\|A(x,t)\|_{L^2(\Sigma)} = \left\{ \int_0^T \int_\Gamma |A(x,t)|^2\ dxdt \right\}^{\frac{1}{2}}\ . \qquad (3.5)$$

The directional derivative $\partial A/\partial n$ is given by formula

$$\frac{\partial A}{\partial n} = \sum_{i=1}^{2} \frac{\partial A}{\partial x_i} \cos(n,x_i)\ , \qquad (3,6)$$

where n is a vector normal to the edge Γ of space Ω

$$\Gamma = \left\{ x_1\ x_2 :\ x_1^2/a^2 + x_2^2/b^2 = 1 \right\}, \qquad (3.7)$$

$$\Omega = \left\{ x_1\ x_2 :\ x_1^2/a^2 + x_2^2/b^2 < 1 \right\}. \qquad (3.8)$$

Therefore the new optimization problem consist in determining the couple $\{A_\varepsilon, b_\varepsilon\}$ satisfying the following relation

$$\inf_{\substack{A \in Y \\ b \in U_{ad}}} J_\varepsilon(A,b) = j_\varepsilon\ . \qquad (3.9)$$

Theorem 2: The problem (3.9) has univocal solution

$$\{A_\varepsilon, b_\varepsilon\} \qquad (3.10)$$

possessing such property that when $\varepsilon = (\varepsilon_1 \varepsilon_2 \varepsilon_3) \to 0$ so

$$j_\varepsilon \to j;\quad A_\varepsilon \to A(b);\quad b_\varepsilon \to b$$

in space Y and U_{ad}, respectively.
Proof of this theorem is given in work [6]. In fact, when A and b will obtain optimum values, so constituent penalties in the modified functional (3.3) will be nulling and

$$J_\varepsilon(A_\varepsilon\ b_\varepsilon) \leqslant J(A(b)\ b) = J(b) = j\ , \qquad (3,11)$$

In further considerations we will treat construction of the optimum couple (3.10) by approximation method of the state function $A(x,t)$ and magnetization $b(x,t)$ by means of the finite element [5, 7, 8].

4. APPROXIMATION OF THE SOLUTION BY MEANS OF THE FINITE ELEMENT

The quality functional (3.3) in the open notation has the form

$$J_\varepsilon(A\ b) = \frac{1}{2}\int_\Omega (A(x,T) - A_d(x))^2 dx + \gamma/2 \int_0^T \int_\Omega b^2(x,t) dxdt +$$

$$+ \frac{1}{2\varepsilon_1} \int_0^T \int_\Omega \left(\frac{\partial}{\partial t} A(x,t) + \frac{1}{\mu} \sum_{i=1}^{2} \frac{\partial^2}{\partial x_i^2} A(x,t) \right)^2 dx\ dt +$$

$$+ \frac{1}{2\varepsilon_2} \int_0^T \int_\Gamma \left(\sum_{i=1}^{2} \frac{\partial}{\partial x_i} A(x,t)\ a_i(x) - b(x,t) \right)^2 dx\ dt + \qquad (4.1)$$

$$+\frac{1}{2\varepsilon_3}\int_{\Omega}(A(x,0)-A_0(x))^2\,dx \quad . \qquad (4.1)$$

Considering that functional (4.1) depends of derivatives of second order in relation to the variable $x=(x_1,x_2)$, it is necessary to apply approximation of the state function and boundary magnetization by means of the second order polynomials $P_h^r(x,t)\in H^2(Q^e)$, $x=(x_1,x_2)$

$$A(x,t)=[P]\{\alpha\} \quad , \qquad (4.2)$$

where

$$[P]=[1,x_1\ x_2\ t\ x_1^2\ x_2^2\ t^2\ x_1x_2\ x_1t\ x_2t] \ ,$$
$$\{\alpha\}=\{\alpha_1\ \alpha_2\ \alpha_3\ \alpha_4\ \alpha_5\alpha_6\ \alpha_7\ \alpha_8\ \alpha_9\ \alpha_{10}\} \quad .$$

Region Q has been divided into M trihedral elements as in Fig. 1

$$Q=\Omega\times(0,T)=\bigcup_{e=1}^{M}Q^{(e)} \qquad (4.3)$$

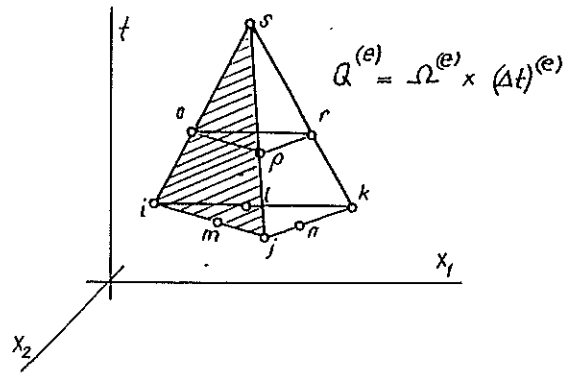

Fig. 1. Configuration of nodes in the element

In the e-th element $Q^{(e)}$ distribution of the state function $A(Q^e)$ is expressed by relation

$$A(Q^e)=[P][G]^{-1}\{A\} \quad \text{or} \qquad (4.4)$$

$$A(Q^e)=[N]\{A\} \quad , \qquad (4.5)$$

where $[G]$ is a square matrix of the order (10 x 10). Its elements are expressed by co-ordinates of nodes $x_{1\beta}$, $x_{2\beta}$, t_β , $\beta=i\ j\ k\ l\ m\ n\ o\ p\ r\ s$; $[N]$ is the vector of shape function

$$[N]=[N_i\ N_j\ N_k\ N_l\ N_m\ N_n\ N_o\ N_p\ N_r\ N_s] \ , \qquad (4.6)$$
$$\{A\}=[A_i\ A_j\ A_k\ A_l\ A_m\ A_mA_n\ A_o\ A_p\ A_r\ A_s] , \qquad (4.7)$$

as well as

$$N_\beta(x_1x_2t)=\frac{1}{\Delta}(a_\beta+b_\beta x_1+c_\beta x_2+d_\beta t+f_\beta x_1^2+$$
$$+g_\beta x_2^2+h_\beta t^2+u_\beta x_1x_2+v_\beta x_1t+w_\beta x_2t) \ , \qquad (4.8)$$

$$\frac{\partial N_\beta}{\partial x_1}=\frac{1}{\Delta}(b_\beta+2f_\beta x_1+u_\beta x_2+v_\beta t) \quad , \qquad (4.9)$$

$$\frac{\partial N_\beta}{\partial x_2}=\frac{1}{\Delta}(c_\beta+2g_\beta x_2+u_\beta x_1+w_\beta t) \quad , \qquad (4.10)$$

$$\frac{\partial N}{\partial t}=\frac{1}{\Delta}(d_\beta+2h_\beta t+v_\beta x_1+w_\beta x_2) \quad , \qquad (4.11)$$

$$\frac{\partial^2N_\beta}{\partial x_1^2}=\frac{2}{\Delta}f_\beta \ ; \ \frac{\partial^2N}{\partial x_2^2}=\frac{2}{\Delta}g_\beta \quad , \qquad (4.12)$$

where Δ is determinant of matrix $[G]$.
Therefore, distribution of the state function $A(x,t)$ and boundary magnetization $b(x,t)$ can be represented in the form

$$A(Q^e)=\sum_\beta N_\beta(x_1x_2t)A_\beta \quad , \qquad (4.13)$$

$$b(\Sigma^e)=\sum_\beta N_\beta(x_1x_2t)b_\beta \quad . \qquad (4.14)$$

According to additive properties of the integral the functional (4.1) will be represented in the form of sum of components determined in $Q^{(e)}$ by the elements

$$J_\varepsilon(A\ b)=\sum_{e=1}^{M}J_\varepsilon^{(e)}(A\ b) \ . \qquad (4.15)$$

where the e-th component of the above sum equals to

$$J_{\varepsilon}^{(e)}(\Lambda\ b) = J_T^{(e)} + J_\gamma^{(e)} + \sum_{i=1}^{3} J_i^{(e)} \quad . \qquad (4.16)$$

Accordingly

$$J_T^{(e)}(\Lambda\ b) = \frac{1}{2}\int_{\Omega e} (\Lambda(x\,T) - 2\Lambda(x\,T)\Lambda_d(x) + \Lambda_d(x)\Lambda_d(x)dx \qquad (4.17)$$

$$J_\gamma^{(e)}(\Lambda, b) = \frac{\gamma}{2}\int_{\Delta t}\int_{\Gamma} b(xt)\ b(x,t)\ dx\ dt\ , \qquad (4.18)$$

$$J_{\varepsilon_1}^{(e)}(\Lambda\ b) = \frac{1}{2\varepsilon_1}\int_{\Delta t}\int_{\Omega} \left(\frac{\partial\Lambda}{\partial t}\frac{\partial\Lambda}{\partial t} + \frac{2}{\mu}\frac{\partial\Lambda}{\partial t}\frac{\partial^2\Lambda}{\partial x_1^2} + \right.$$

$$\left. + \frac{1}{\mu}\frac{\partial^2\Lambda}{\partial x_1^2}\frac{\partial^2\Lambda}{\partial x_1^2} + \frac{2}{\mu}\frac{\partial^2\Lambda}{\partial x_2^2} + \frac{1}{\mu}\frac{\partial^2\Lambda}{\partial x_2^2}\frac{\partial^2\Lambda}{\partial x_2^2}\right)dx\ dt\ , \qquad (4.19)$$

$$J_{\varepsilon_2}^{(e)}(\Lambda\ b) = \frac{1}{2\varepsilon_2}\int_{\Delta t}\int_{\Gamma} (a_1\ a_1\frac{\partial\Lambda}{\partial x_1}\frac{\partial\Lambda}{\partial x_1} +$$

$$+ 2a_1\ a_2\frac{\partial\Lambda}{\partial x_1}\frac{\partial\Lambda}{\partial x_2} + a_2\ a_2\frac{\partial\Lambda}{\partial x_2}\frac{\partial\Lambda}{\partial x_2} - 2\ a_1\frac{\partial\Lambda}{\partial x_1}\ b\ +$$

$$- 2a_2\frac{\partial\Lambda}{\partial x_2}\ b + b(x,t)\ b(x,t))\ dx\ dt\ , \qquad (4.20)$$

$$J_{\varepsilon_3}^{(e)}(\Lambda) = \frac{1}{2\varepsilon_3}\int_{\Omega} (\Lambda(x,0)\Lambda(x,0) - 2\Lambda(x,0)\Lambda_o(x) +$$

$$+ \Lambda_o(x)\Lambda_o(x))\ dx \quad . \qquad (4.21)$$

By approximation of each of this components we obtain

$$J_T^{(e)}(\{\Lambda\}) = \frac{1}{2}\{\Lambda\}^T\ [C_1]\{\Lambda\} - \{\Lambda\}^T\ [C_1]\ \{\Lambda_d\} +$$

$$+ \frac{1}{2}\{\Lambda_d\}^T[C_1]\ \{\Lambda_d\}\ , \qquad (4.22)$$

where matrix $[C]$ is a square matrix of the order $(M \times M)$

$$[C_1] = \int_{\Omega} [N]^T\ [N]\ (T)\ dx \quad , \qquad (4.23)$$

$$J_\gamma^{(e)}(\{b\}) = \frac{\gamma}{2}\{b\}^T\ [C_2]^{(e)}\ \{b\}\ , \qquad (4.24)$$

where

$$[C_2]^{(e)} = \int_{\Delta t}\int_{\Gamma} [N]^T\ [N]\ dx\ dt\ , \qquad (4.25)$$

$$J_{\varepsilon_1}^{(e)}(\{\Lambda\}) = \frac{1}{2\varepsilon_1}\{\Lambda\}^T\ [D]^{(e)}\ \{\Lambda\}\ , \qquad (4.26)$$

where

$$[D]^{(e)} = \int_{\Delta t}\int_{\Omega} \frac{\partial}{\partial t}[N]^T\frac{\partial}{\partial t}[N] +$$

$$+ \frac{1}{\mu}(2\frac{\partial}{\partial t}[N]^T\frac{\partial^2}{\partial x_1^2}[N] + \frac{\partial^2}{\partial x_1^2}[N]^T\frac{\partial^2}{\partial x_1^2}[N] +$$

$$+ 2\frac{\partial^2}{\partial x_1^2}[N]^T\frac{\partial^2}{\partial x_2^2}[N] + \frac{\partial^2}{\partial x_2^2}[N]^T\frac{\partial^2}{\partial x_2^2}[N])\,dx\ dt\ ; \qquad (4.27)$$

$$J_{\varepsilon_2}^{(e)}(\{\Lambda\}\{b\}) = \frac{1}{2\varepsilon_2}\{\Lambda\}^T\ [E]^{(e)}\{\Lambda\} +$$

$$- \frac{1}{2\varepsilon_2}\{\Lambda\}^T\ [F]^{(e)}\{b\} + \frac{1}{2\varepsilon_2}\{b\}^T\ [C]^{(e)}\{b\}\ , \qquad (4.28)$$

where

$$[E]^{(e)} = \int_{\Delta t}\int_{\Gamma} (a_1^2\frac{\partial}{\partial x_1}[N]^T\frac{\partial}{\partial x_1}[N] +$$

$$+ a_1a_2\frac{\partial}{\partial x_1}[N]^T\frac{\partial}{\partial x_2}[N] + a_2^2\frac{\partial}{\partial x_2}[N]^T\frac{\partial}{\partial x_2}[N])dx\ dt, \qquad (4.29)$$

$$[F]^{(e)} = \int_{\Delta t}\int_{\Omega} (a_1\frac{\partial}{\partial x_1}[N]^T[N] + a_2\frac{\partial}{\partial x_2}[N]^T[N])dx\ dt\ , \qquad (4.30)$$

$$[C_1]^{(e)} = \int_{\Delta t}\int_{\Omega} [N]^T [N](x,t)\, dx\, dt \quad , \qquad (4.31)$$

as well as

$$J^{(e)}_{\varepsilon 3}(\{A\}) = \frac{1}{2\varepsilon_3}\{A\}^T [C_3]\{A\} - \frac{1}{\varepsilon_2}\{A\}^T [C_3]^{(e)}\{A_o\} + \frac{1}{2\varepsilon_3}\{A_o\}^T [C_3]^{(e)}\{A_o\} \quad , \qquad (4.32)$$

where matrix $[C_3]^{(e)}$ equals

$$[C_3]^{(e)} = \int_{\Omega} [N]^T [N](0)\, dx \quad . \qquad (4.33)$$

The functional (3.3); (4.1) in the descrete space $(Y \times U)_h^{r=2}$ is precisely convex and radially divergent. Therefore, condition of its extreme assumes the form

$$\frac{\partial}{\partial\{A\}} J_{\varepsilon}(\{A\}\{b\}) = 0 \quad , \qquad (4.34)$$

$$\frac{\partial}{\partial\{b\}} J_{\varepsilon}(\{A\}\{b\}) = 0 \quad , \qquad (4.35)$$

Derivatives of seperate components: (4.22), (4.24), (4.26), (4.28), (4.32) in relation to vectors $\{A\}$ and $\{b\}$ are equal respectively to

$$\frac{\partial}{\partial\{A\}} J^{(e)}_T(\{A\}\{b\}) = [C_1]^{(e)}\{A\} - [C_1]^{(e)}\{A_d\} \qquad (4.36)$$

$$\frac{\partial}{\partial\{b\}} J^{(e)}_T(\{A\}\{b\}) = 0 \quad , \qquad (4.37)$$

$$\frac{\partial}{\partial\{A\}} J^{(e)}_{\gamma}(\{A\}\{b\}) = 0 \quad , \qquad (4.38)$$

$$\frac{\partial}{\partial\{b\}} J^{(e)}_{\gamma}(\{A\}\{b\}) = C_2^{(e)} b \quad , \qquad (4.39)$$

$$\frac{\partial}{\partial\{A\}} J^{(e)}_{\varepsilon 1}(\{A\}\{b\}) = \frac{1}{\varepsilon_1} [D]^{(e)}\{A\} \quad , \qquad (4.40)$$

$$\frac{\partial}{\partial\{b\}} J^{(e)}_{\varepsilon 1}(\{A\}\{b\}) = 0 \quad , \qquad (4.41)$$

$$\frac{\partial}{\partial\{A\}} J^{(e)}_{\varepsilon 2}(\{A\}\{b\}) = \frac{1}{\varepsilon_2} [E]^{(e)}\{A\} - \frac{1}{\varepsilon_2} [F]^{(e)}\{b\} \quad , \qquad (4.42)$$

$$\frac{\partial}{\partial\{b\}} J^{(e)}_{\varepsilon 2}(\{A\}\{b\}) = -\frac{1}{\varepsilon_2} [F]^{(e)}\{b\} \quad , \qquad (4.43)$$

$$\frac{\partial}{\partial\{A\}} J^{(e)}_{\varepsilon 3}(\{A\}\{b\}) = \frac{1}{\varepsilon_3} [C_3]^{(e)}\{A\} - \frac{1}{\varepsilon_3} [C_3]^{(e)}\{A_o\} \qquad (4.44)$$

$$\frac{\partial}{\partial\{b\}} J^{(e)}_{\varepsilon 3}(\{A\}\{b\}) = 0 \quad . \qquad (4.45)$$

Conditions (4.34) and (4.35) give the set of equations in relation to vectors of state $\{A\}$ and magnetization $\{b\}$. These equations assume the following form for the e-th element

$$\left([C_1]^{(e)} + \frac{1}{\varepsilon_1}[D]^{(e)} + \frac{1}{\varepsilon_2}[E]^{(e)} + \frac{1}{\varepsilon_3}[C_3]^{(e)}\right)\{A\} - \frac{1}{\varepsilon_2}[F]^{(e)}\{b\} = ([C_1])^{(e)}\{A_d\} + \frac{1}{\varepsilon_3}([C_3])^{(e)}\{A_o\} \quad , \qquad (4.46)$$

$$\frac{1}{\varepsilon_2}([F])^{(e)}\{A\} - (\gamma[C_2]^{(e)} + \frac{1}{\varepsilon_2}[C_4]^{(e)})\{b\} = 0 \quad . \qquad (4.47)$$

Assembling partial matrices along all elements e=1,2, ...,11 we obtain the set of equations

$$[C]\{A\} - \frac{1}{\varepsilon_2}[F]\{b\} = \{f\} \quad , \qquad (4.48)$$

$$-\frac{1}{\varepsilon_2}[F]\{A\} + [D]\{b\} = \{0\} \quad , \qquad (4.49)$$

where

$$[C] = \sum_{e=1}^{M} [C_1]^{(e)} + \frac{1}{\varepsilon_1}[D]^{(e)} + \frac{1}{\varepsilon_2}[E]^{(e)} + \frac{1}{\varepsilon_3}[C_3]^{(e)}) \quad , \tag{4.50}$$

$$[F] = \sum_{e=1}^{M} [F]^{(e)} \quad , \tag{4.51}$$

$$[D] = \sum_{e=1}^{M} (\gamma [C_2]^{(e)} + \frac{1}{\varepsilon_2}[C_4]^{(e)}) \quad , \tag{4.52}$$

$$\{f\} = \sum_{e=1}^{M} ([C_1]^{(e)}\{A_d\} + \frac{1}{\varepsilon_3}[C_3]^{(e)}\{A_o\}) \quad , \tag{4.53}$$

Further, the set (4.48) and (4.49) will be recorded in the form of a single matrix equation

$$\begin{bmatrix} [C] & -\frac{1}{\varepsilon_2}[F] \\ -\frac{1}{\varepsilon_2}[F] & [D] \end{bmatrix} \begin{Bmatrix} \{A\} \\ \{b\} \end{Bmatrix} = \begin{Bmatrix} \{f\} \\ \{0\} \end{Bmatrix} \quad , \tag{4.54}$$

$$\begin{Bmatrix} \{A\} \\ \{b\} \end{Bmatrix} = \begin{bmatrix} [C] & -\frac{1}{\varepsilon_2}[F] \\ -\frac{1}{\varepsilon_2}[F] & [D] \end{bmatrix}^{-1} \begin{Bmatrix} \{f\} \\ \{0\} \end{Bmatrix} \quad . \tag{4.55}$$

Vector (4.55) represents the inquired solution of the stated problem of optimization of the boundary magnetization. The state vector $\{A\}$ determines distribution of the vectorial potential in the region $Q = \Omega \times (0,T)$ in its discrete nodes.
Vector $\{b\}$ determines distribution of magnetic induction in points located on the edge of the eliptic cylinder $\Sigma = \Gamma \times (0,T)$. This vector causes that after time (T) distribution of the magnetic $\{A(T)\}$ is optimaly near to the present distribution $\{A_d\}$. This proximity is understood as the essence of the quality criterion (3.3), (4.1).
Penalty factors γ , ε_i $(i=1,2,3)$ should be selected beforehand so as to avoid domination of the functional (2.11) by penalty functionals.

5. CONCLUDING REMARKS

The represented method of penalty functionals makes it possible to substitute in an effective manner the problem of optimization with limitations by the problem without limitations. This simplifies calculations connected with construction of the functional extreme point. However, substitution of the state equation (2.5) as basic limitation by functional (4.19) in the norm $L^2(Q)$ involves necessity of approximation by an element of higher order, at least of second order, and this is connected with some additional calculations.
Selection of factors: of regularization γ and of penalty ε_i $(i=1,2,3)$ requires certain experience in calculations and is performed individually to the problem.
The represented algorithm of determining the optimum boundary magnetization with final observation $A(x,T)$ is executed on a digital computer in language FORTRAN. The program of calculations is actually in cause of realization.

6. REFERENCES

1. Adams R.A.: Sobolev spaces. Academic Press, New York, 1975.

2. Balakrishnan A.Y.: On a new computing technique in optimum control. SIAM J. on Control, Vol. 6, Nr 2, 1968.

3. Johnk T.A.: Engineering Electromagnetic Fields and Waves. New York, 1975.

4. Krzemiński S.K.: Identyfikacja impedancji obciążenia niejednorodnej linii długiej. Archiw.Elektrotech. Nr 2, 1978.

5. Krzemiński S.K.: Application of the optimization of an Elliptic System, in Proc. Symposium on Simulation of Control Systems, Vienna 1978.

6. Lions J.L.: Contrôle optimal de Systemès gouvernés par des équations aux derivés partielles. Dunad, 1968.

7 . Malanowski K.: On triangle approximation of domain in discrete-time Ritz-Galerkin type method for optimum control of parabolic system. Archiwum Automatyki i Telemechaniki, Nr 3. 1977.

8 . Zienkiewicz O.C.: The Finite Element Method in Engineering Science. McGraw Hill, London 1971.

9 . Harley P.J., Mitchell A.R.: Finite Element collocation Method for The Exact Control of a Parabolic Problem. Int. J. for Numerical Meth. Vol. 11,1977.